NAVAL POSTGRADUATE SCHOOL

MONTEREY, CALIFORNIA

THESIS

MODELING AND MODEL IDENTIFICATION OF AUTONOMOUS UNDERWATER VEHICLES

by

Jose Alberti

June 2015

Thesis Advisor: Noel du Toit
Second Reader: Douglas Horner

Approved for public release; distribution is unlimited

THIS PAGE INTENTIONALLY LEFT BLANK

REPORT DOCUMENTATION PAGE

Form Approved OMB No. 0704-0188

1. AGENCY USE ONLY *(Leave blank)*	**2. REPORT DATE** June 2015	**3. REPORT TYPE AND DATES COVERED** Master's Thesis

4. TITLE AND SUBTITLE
MODELING AND MODEL IDENTIFICATION OF AUTONOMOUS UNDERWATER VEHICLES

5. FUNDING NUMBERS

6. AUTHOR(S) Jose Alberti

7. PERFORMING ORGANIZATION NAME(S) AND ADDRESS(ES)
Naval Postgraduate School
Monterey, CA 93943-5000

8. PERFORMING ORGANIZATION REPORT NUMBER

9. SPONSORING /MONITORING AGENCY NAME(S) AND ADDRESS(ES)
N/A

10. SPONSORING/MONITORING AGENCY REPORT NUMBER

11. SUPPLEMENTARY NOTES The views expressed in this thesis are those of the author and do not reflect the official policy or position of the Department of Defense or the U.S. Government. IRB Protocol number ____N/A____.

12a. DISTRIBUTION / AVAILABILITY STATEMENT
Approved for public release; distribution is unlimited

12b. DISTRIBUTION CODE

13. ABSTRACT (maximum 200 words)

As autonomous underwater vehicles (AUVs) are deployed in more complex operational scenarios (e.g., multi-vehicle operations or information gathering in cluttered littoral zones), accurate control of these platforms is of particular importance. However, the design of accurate controllers and these complex systems in general require accurate models.

This research is focused on the identification of rigid body and hydrodynamic modeling parameters of the THAUS (a modified SeaBotix vLBV300) and the Hydroid REMUS100 AUVs. A hydrodynamic model is adopted that accounts for vehicle-specific properties, including symmetry and anticipated flow properties. An experimental setup, based on a quadrifilar pendulum, is developed to measure the moments of inertia of the vehicle. System identification techniques, based on Recursive Least Squares estimation with modifications for learning the parameters of dynamic systems, are applied in two approaches to learn the parametric models of the platforms: an individual channel excitation approach and a free decay pendulum test. The former is applied to THAUS, which can excite the system in individual channels in four degrees of freedom. These results are verified in the free decay pendulum setup, which has the advantage that the approach is independent of the platform actuation. The latter test is also applied to the REMUS AUV.

14. SUBJECT TERMS
autonomous and underwater vehicles, hydrodynamic modeling, system identification, model learning

15. NUMBER OF PAGES
87

16. PRICE CODE

17. SECURITY CLASSIFICATION OF REPORT	**18. SECURITY CLASSIFICATION OF THIS PAGE**	**19. SECURITY CLASSIFICATION OF ABSTRACT**	**20. LIMITATION OF ABSTRACT**
Unclassified	Unclassified	Unclassified	UU

NSN 7540-01-280-5500

Standard Form 298 (Rev. 2-89)
Prescribed by ANSI Std. 239-18

THIS PAGE INTENTIONALLY LEFT BLANK

Approved for public release; distribution is unlimited

MODELING AND MODEL IDENTIFICATION OF AUTONOMOUS UNDERWATER VEHICLES

Jose Alberti
Lieutenant Junior Grade, Peruvian Navy
B.S., Peruvian Naval Academy, 2009

Submitted in partial fulfillment of the
requirements for the degree of

MASTER OF SCIENCE IN MECHANICAL ENGINEERING

from the

NAVAL POSTGRADUATE SCHOOL
June 2015

Author: Jose Alberti

Approved by: Noel du Toit
Thesis Advisor

Douglas Horner
Second Reader

Garth V. Hobson
Chair, Department of Mechanical and Aerospace Engineering

THIS PAGE INTENTIONALLY LEFT BLANK

ABSTRACT

As autonomous underwater vehicles (AUVs) are deployed in more complex operational scenarios (e.g., multi-vehicle operations or information gathering in cluttered littoral zones), accurate control of these platforms is of particular importance. However, the design of accurate controllers and these complex systems in general require accurate models.

This research is focused on the identification of rigid body and hydrodynamic modeling parameters of the THAUS (a modified SeaBotix vLBV300) and the Hydroid REMUS100 AUVs. A hydrodynamic model is adopted that accounts for vehicle-specific properties, including symmetry and anticipated flow properties. An experimental setup, based on a quadrifilar pendulum, is developed to measure the moments of inertia of the vehicle. System identification techniques, based on Recursive Least Squares estimation with modifications for learning the parameters of dynamic systems, are applied in two approaches to learn the parametric models of the platforms: an individual channel excitation approach and a free decay pendulum test. The former is applied to THAUS, which can excite the system in individual channels in four degrees of freedom. These results are verified in the free decay pendulum setup, which has the advantage that the approach is independent of the platform actuation. The latter test is also applied to the REMUS AUV.

THIS PAGE INTENTIONALLY LEFT BLANK

TABLE OF CONTENTS

LIST OF FIGURES

LIST OF TABLES

THIS PAGE INTENTIONALLY LEFT BLANK

LIST OF ACRONYMS AND ABBREVIATIONS

AUV	Autonomous Underwater Vehicle
CAD	Computer-Aided Design
DOF	Degree of Freedom
EOM	Equation of Motion
FDP	Free Decay Pendulum
GE	Gradient Estimator
IMU	Inertial Measurement Unit
NN	Neural Network
PE	Persistence of Excitation
RLSE	Recursive Least Squares Estimation
RMSE	Root Mean Square Error
ROV	Remotely Operated Vehicle
SCE	Single Channel Excitation
UUV	Unmanned Underwater Vehicle

THIS PAGE INTENTIONALLY LEFT BLANK

ACKNOWLEDGMENTS

To my family, because the warm feelings coming from them are the fuel that drove me to where I am today. I will always be grateful for that.

To Noel Du Toit, for helping me to push this project even when I told him from day one that my experience in the field was pretty close to zero, and to Douglas Horner, for taking the time to review this project.

To Karima and Rene, without you two I could probably have learned something during classes, but who wants to do that anyway.

To Joe and Aric, the older brothers I never had. I could have not survived two years of graduate school in a foreign country without the fun times we had together. Living in California would not have been the same without getting to know you two.

And to Carolyn, for absolutely everything.

THIS PAGE INTENTIONALLY LEFT BLANK

I. INTRODUCTION

Since its inception, diving operations have been closely related to the naval profession with operations like the recovery of sunken values, inspection and maintenance, and the search navigation of underwater barricades. It is also considered to be one of the most dangerous habitats for humans due to hazards such as decompression sickness, exposure to very high pressures, limited diving time, limited visibility, etc. Recent technological developments have eased the burden on divers for safer and more efficient operations. One example is the introduction of underwater Remotely Operated Vehicles (ROV) aiding or even sometimes replacing the diver in underwater operations. The natural extension of this technology is the introduction of automated capabilities for performing complex underwater tasks, potentially with humans-in-the-loop, to accomplish more complex tasks through the collaboration of robots and humans (see Figure 1). This requires these vehicles to share its operational environment with human divers as well as operate close to other objects (e.g., the sea floor, vessels, and other underwater vehicles). This in turn requires precise control at a level not needed before, to operate safely in an environment with large disturbances and where sensing and communication is inherently limited. That is when accurate modeling is needed.

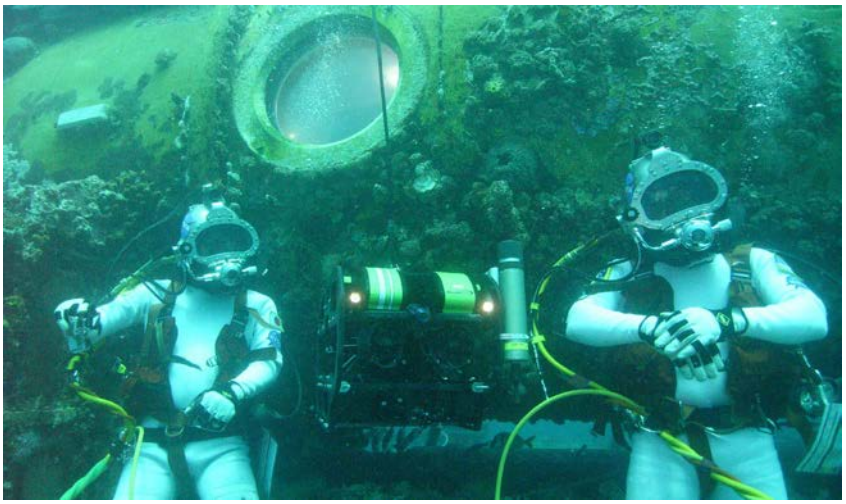

Figure 1. THAUS AUV during diving operations at NASA Aquarius Reef Base.

A model of the dynamics of the underwater platform is needed for accurate control and state estimation. However, obtaining accurate models of underwater vehicles is extremely challenging due to hydrodynamic effects such as damping and added mass coefficients for all six degrees of freedom. These effects are highly coupled and hard to calculate analytically or computationally. As will be shown, general parametric models contain more than 200 unknown parameters that must be calculated or estimated. This problem is further complicated by the fact that vehicle configuration changes result in changes in the dynamic model. Thus, methods to capture these models through experimentation are desired.

The focus of this research is developing experimental methods to obtain the hydrodynamic parameters that model the motion of two classes of underwater vehicles, using inexpensive, flexible methods.

A. LITERATURE REVIEW

Several steps must be addressed in order to obtain an accurate model of the dynamics of the AUV. First, a parametric model of the rigid body dynamics under hydrodynamic forces is needed before the model parameters can be estimated. The mass and inertia properties, in addition to the hydrodynamic coefficients must be identified. Several techniques exist in order to address this task.

Parametric models that capture the dynamics of the vehicle are needed in order to design, simulate and validate controllers. A general model of the dynamics of a rigid body moving in the presence of hydrodynamic forces has been well studied over the last 25 years, as presented by Fossen [1]. This model captures all the elements of the six degrees of freedom (DOF) motion of the body. The presented generic model can be applied to all marine vehicles, surface or underwater. These generalized equations of motion (EOMs) can be significantly simplified depending on the properties of the rigid body. For example, Prestero [2] and Doherty [3], while working on the REMUS AUV, assumed symmetry in the *xy-plane* and *xz-plane*, yielding a particular set of EOMs that can be applied to the REMUS. Similarly, Weiss [4] and Eng *et al.* [5, 6] assumed three planes of symmetry (*xy*, *xz* and *zy*) and uncoupled motion for the open-frame hovering

AUVs, eliminating some of the terms that were still present on the simplified version Prestero and Doherty used.

With this parametric model that captures the dynamics of underwater vehicles in hand, the next steps are the identification of the rigid body (mass and inertia) and hydrodynamic (added mass, fluid damping effects and buoyancy) parameters.

For simple body shapes, a good approximation of the inertia properties of underwater vehicles can be obtained by assuming homogeneous distribution of mass and simplifying the shape of the vehicle [2, 4]. However, other methods are available that result in more accurate estimates. Computer-Aided Design (CAD) software is capable of calculating the moment of inertia of a rigid body [5], even when it is composed of different materials. Although it is a good approach, the result will only be as accurate as the CAD model reflects the reality. Some components may be more complex (e.g., a sonar or other sensors) for which accurate CAD models may not exist, resulting in inaccuracies. Additionally, a change in the configuration of the vehicle (e.g., a change in the sensor placement) will result in a change in the moment of inertia, which would involve updating the CAD model to obtain the new result. For vehicles like the THAUS AUV, for which versatility is key feature, this is inconvenient and lowers overall confidence in the estimated inertias. Experimental methods can be used to identify these same properties. Particularly, using multi-filar pendulums [7, 8], the moment of inertia about several planes principal axes can be found, due to the relationship with the pendulum's period of oscillation. This technique will be further explored in this work.

When rigid bodies are submerged in a fluid and accelerate (i.e., forced motion), the inertia of the surrounding fluid must be overcome as well as the inertia of the vehicle. This is known as the added mass component of the hydrodynamic model. This property is normally treated as a function of the geometry only [1-6, 9-12], including in the author of this thesis[1]. Keeping with this convention, two options for the identification of these properties exist: calculation or experimental identification. Doherty [3] used Blevins [14] and Newman's [15] empirical equations of the added mass of a cylindrical body to

[1] A recent study suggests that the added mass is additionally a function of the acceleration of the body through the fluid [13]. This should be explored in follow-on work.

calculate the axial and crossflow added mass, which is a good approximation for the REMUS AUV. Eng *et al*. [5] used the specialized CAD software WAMIT (WaveAnalisysMIT) to calculate these coefficients. Again, these methods are only as good as the CAD models that exist for the platforms. As will be shown later in this chapter, the THAUS AUV has very complex geometry, for which these techniques cannot be readily applied with high confidence. The experimental identification of the added mass properties requires treating these coefficients as unknowns and applying system identification techniques to obtain them [4, 6, 12]. This is the method that will be explored in this work.

Similarly, the drag, or damping, coefficients can be calculated or experimentally identified. Due to the fact that not all underwater vehicles have body shapes that allows this calculation [3], experimental identification is the preferred method [2, 4, 6, 10-12, 16]. This becomes a challenging task due to the highly coupled nature of the damping effects, especially when dealing with open-frame vehicles like the THAUS AUV.

As mentioned, the experimental identification of these parametric models requires the estimation of the various unknowns from measured vehicle responses. Several methods have been explored for the experimental identification of hydrodynamic coefficients of marine vehicles. Tow tank testing has been around for a long time [2, 16] to identify these coefficients. The appropriate use of the facilities and equipment has been used to successfully identify the coefficients in the six DOFs. However, as with the moment of inertia, a change in the configuration could change these properties significantly. Furthermore, a tow-tank facility is not always available. A more convenient approach is to use the actuators of the platform itself to excite the vehicle [4]. However, while this is possible for vehicles like the THAUS, the REMUS AUV cannot excite all its DOFs individually by using just its actuators. As an alternative, constrained pendulum motion has also been used to excite scaled models and identify the desired parameters [6]. Yet, as the vehicles become more versatile, allowing customization for different missions, new identification methods must be explored, like online identification [4] and adaptive methods [12].

The identification task consists in fitting a mathematical model to the obtained vehicle response data. Regression tools are widely used for this purpose, such as the Least Squares Estimation [6, 9, 11, 12], where the data is processed after it is obtained (i.e., off-line). A more versatile approach is the use of recursive tools, such as Recursive Least Square Estimators, Gradient Estimators and Neural Networks [4], which estimate the parameters of the model as new information becomes available (i.e., online). Additionally, adaptive control techniques are available [12] that can react to changes in the payload in order to tune the existing model, further leveraging these on-line model learning tools. There are additional considerations in order to use the latter methods, like the richness of the input signal [4, 17] that need to be address to get accurate results. This methodology will be explored further in this thesis.

B. PLATFORMS

The model learning techniques developed in this research will be applied to two different vehicles: the THAUS AUV and the REMUS AUV. These two platforms are fundamentally different, not only in their dynamical capabilities, but in the mission they are used for.

1. THAUS: Tethered Hovering Autonomous Underwater System

The THAUS AUV is a modified vLBV300 miniROV, manufactured by TELEDYNE SeaBotix Inc. in San Diego, California. A tether transmits power and information to control the vehicle, which can be controlled via a joystick interface. Figure 2 shows an example of the configuration of the vLBV300.

Figure 2. Standard SeaBotix vLVB300 miniROV

The standard model comes with six brushless DC thrusters, four of them placed to control planar motion and whose angles can be manually changed prior to operation, and the remaining two are fixed to control vertical motion. This configuration controls the vehicle in five degrees of freedom (DOFs): *surge*, *sway*, *heave*, *roll* and *yaw*, although only four through the joystick interface (*surge*, *sway*, *heave* and *yaw*). The versatility of the vehicle allows the use of a wide arrange of sensors for different applications, including a 650 line high resolution camera with tilt control in 180 degrees, side cameras and sonars. For physical intervention, the vehicle comes with a grabber arm. Table 1 summarizes the general characteristics of the vLBV300.

Table 1. General characteristics of the standard vLBV300 MiniROV, from [18]

Depth Rating	300 m
Length	625 mm
Width	390 mm
Height	390 mm
Diagonal	551 mm
Weight in air	18.1 kg

The Center of Autonomous Vehicle Research (CAVR) has been working on the automation of the vLBV300 by adding sensors capable of estimate the states of the vehicle: an Inertial Navigation System (INS), a Global Positioning System (GPS) and a Doppler Velocity Log (DVL). Additionally, the THAUS AUV has dual forward-looking sonars and a sideways-mounted microbathymetry sonar, allowing accurate environment mapping, feature-based navigation, and obstacle avoidance. Figure 3 shows the updated configuration of the THAUS AUV. A control interface has also been developed that allows fully autonomous operation of the vehicle, in addition to traditional tele-operation control.

Due to its hovering ability, this vehicle is meant to be a diver aid, and it is also able to participate in inspection and mapping operations.

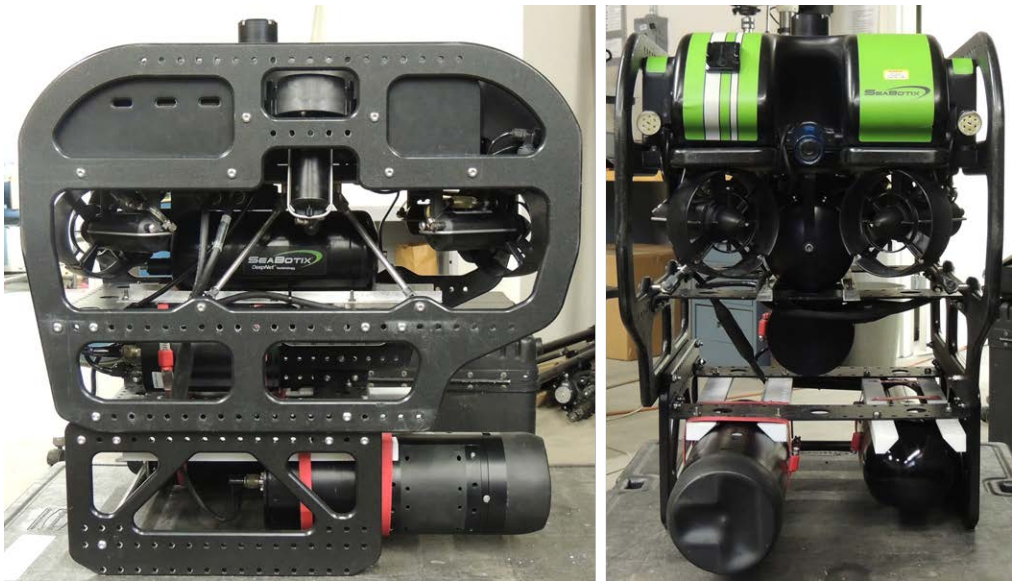

Figure 3. THAUS AUV: Tethered Hovering Autonomous Underwater System

2. REMUS 100: Remote Environmental Measuring Unit

The REMUS is an underwater vehicle manufactured by Hydroid Inc. Its hull shape is given by the Myring hull equations [2], giving it a low drag coefficient for its diameter. Figure 4 shows the shape of the Standard REMUS AUV.

Figure 4. Standard Hydroid REMUS 100

The REMUS AUV uses a single DC brushless motor to power a 3 bladed propeller and impulse the vehicle in the *surge* DOF. A summary of the general characteristics of the vehicle is shown in Table 2.

Table 2. General characteristics of the REMUS AUV, from [19]

Diameter	190 mm
Length	1600 mm
Weight	38.5 kg
Trim weight	1 kg
Maximum operating depth	100 m
Endurance	8-10 hours for a typical mission
Velocity Range	Up to 2.3 m/s

The AUV is designed to move very efficiently in the surge (forward-backward) direction and controls heading and pitch through control surfaces. As a result, the vehicle cannot control heave, sway, pitch, roll, or yaw independently. This is a fundamental difference between the THAUS and REMUS AUVs: while THAUS is a hovering vehicle, the REMUS AUV needs to use its propeller constantly.

Due to its long endurance, the REMUS AUV is used for marine research and exploration.

C. SCOPE AND OBJECTIVES

The main objectives of the research are:

- Derive a model that satisfies the dynamics of the studied vehicles.
- Investigate experimental techniques to learn these dynamic models.
- Experimentally identify the physical and hydrodynamic properties of the parametric models for each vehicle.

To accomplish these objectives, the following tasks were executed:

- Simplify the generalized equations of motion for marine vehicles.
- Experimentally identify the mass and inertia properties of each vehicle.

- Investigate appropriate system identification techniques to learn these dynamic models.
- Use the single channel excitation (SCE) technique to identify the hydrodynamic coefficients of the EOMs for vehicles that can independently excite motion degrees of freedom.
- Use the free decay pendulum (FDP) technique to identify the hydrodynamic coefficients of the EOMs for vehicles that cannot excite motion degrees of freedom independently.

II. HYDRODYNAMIC MODELING

Dynamics of rigid bodies is a well-studied problem. However, submerged bodies have some unique dynamic properties. This chapter will give the lector an inside on the modeling of submerged bodies.

A. RIGID BODY MODELING

The first step of the modeling task is obtaining the equations of motion (EOMs). This chapter will give an overview of the steps that this task requires. For a more detailed explanation, refer to chapter two of Fossen [1].

It is desirable to derive the equations of motion from an arbitrary point located on the body-fixed coordinate frame to take advantage of the geometry of the vehicles. In order to simplify the EOMs, and also because the hydrodynamic and kinematic forces and moments are defined in this coordinate frame. Figure 5 illustrates the motion of an arbitrary rigid body.

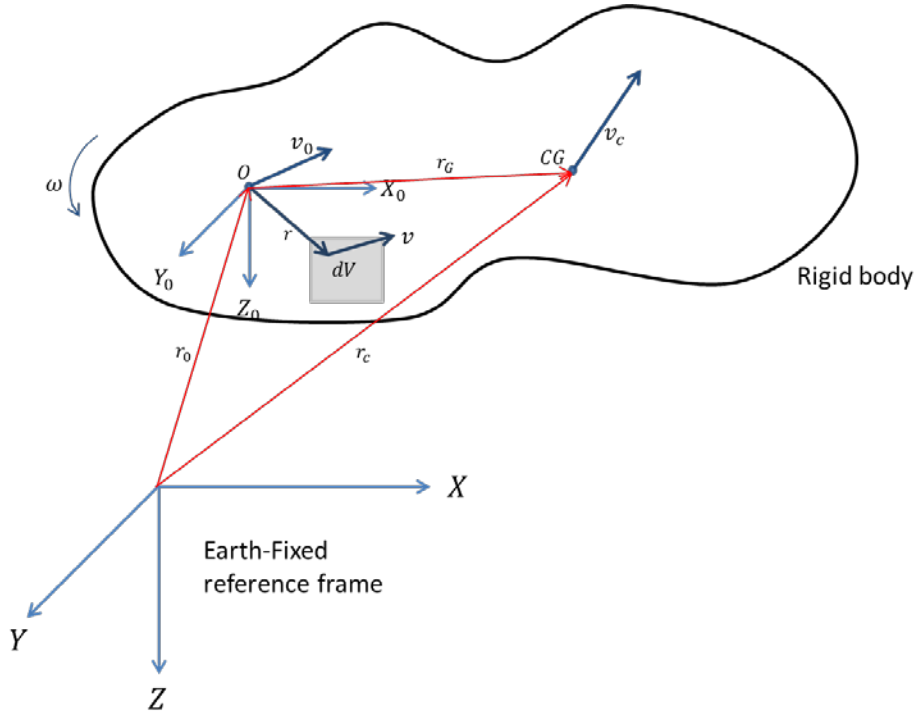

Figure 5. Example of a rigid body motion

A reference frame for the inertial coordinate systems is needed. In practice, it is safe to approximate an earth fixed reference as inertial, since the forces and moments due to the motion of the earth can be neglected in most marine applications.

1. Translational motion

For a body moving in an inertial reference frame, its translation can be computed in a body-fixed coordinate frame as

$$m(\dot{v}_0 + \omega \times v_0 + \dot{\omega} \times r_G + \omega \times (\omega \times r_G)) = f_0 \tag{1}$$

where, in addition to the vectors defined in Figure 5, f is the forces acting on the body. The subscript *o* refers to an arbitrary placed body-fixed frame of reference. It is convenient to choose the origin of this frame to coincide with the body's center of gravity, which allows equation (1) to be simplified to

$$m(\dot{v}_C + \omega \times v_C) = f_C \tag{2}$$

where the subscript *c* refers to the body-fixed frame of reference placed to coincide with the center of gravity.

2. Rotational Motion

Analogously, the rotational motion of a rigid body can be computed in the body-fixed coordinate frame as

$$\mathbf{I}_0 \dot{\omega} + \omega \times (\mathbf{I}_0 \omega) + m r_G \times (\dot{v}_0 + \omega \times v_0) = \mathbf{m}_0 \tag{3}$$

where $\mathbf{m}$ is the moment vector and $\mathbf{I}$ is the inertia tensor, which will be discussed in more detail in Section A of Chapter IV. By choosing the origin of the body-fixed frame to be the same as the center of gravity, equation (3) reduces to

$$\mathbf{I}_C \dot{\omega} + \omega \times (\mathbf{I}_C \omega) = \mathbf{m}_C . \tag{4}$$

3. Vector Equations

The above equations can be written in vector form to include the full six degrees of freedom of a rigid body. Let

$$
\begin{array}{ccccc}
f_0 & = & \tau_1 & = & [X,Y,Z]^T \\
\mathbf{m}_0 & = & \tau_2 & = & [K,M,N]^T \\
v_0 & = & \upsilon_1 & = & [u,v,w]^T \\
\omega & = & \upsilon_2 & = & [p,q,r]^T \\
r_G & & = & & [x_G,y_G,z_G]^T
\end{array}.
$$

Substituting these definitions into equations (1) and (3) yields

$$
\begin{aligned}
&m[\dot{u}-vr+wq-x_G(q^2+r^2)+y_G(pq-\dot{r})+z_G(pr+\dot{q})] && = X \\
&m[\dot{v}-wp+ur-y_G(r^2+p^2)+z_G(qr-\dot{p})+x_G(qp+\dot{r})] && = Y \\
&m[\dot{w}-uq+vq-z_G(p^2+q^2)+x_G(rp-\dot{q})+y_G(rq+\dot{p})] && = Z \\
&I_x\dot{p}+(I_z-I_y)qr-(\dot{r}-pq)I_{xy}+(r^2-q^2)I_{yz}+(pr-q)I_{xy} \\
&\qquad +m[y_G(\dot{w}-uq+vp)-z_G(\dot{v}-wp+ur)] && = K \\
&I_y\dot{q}+(I_x-I_z)rp-(\dot{p}+qr)I_{xy}+(p^2-r^2)I_{zx}+(qp-\dot{r})I_{yz} \\
&\qquad +m[z_G(\dot{u}-vr+wq)-x_G(\dot{w}-uq+vp)] && = K \\
&I_z\dot{r}+(I_y-I_x)pq-(\dot{q}+rp)I_{yz}+(q^2-p^2)I_{xy}+(rq-\dot{p})I_{zx} \\
&\qquad +m[x_G(\dot{v}-wp+ur)-y_G(\dot{u}-vr+wq)] && = N
\end{aligned}. \qquad (5)
$$

These expressions can be compiled in a single equation of the form

$$
\mathbf{M}_{RB}\dot{\upsilon}+\mathbf{C}_{RB}(\upsilon)\upsilon=\tau_{RB} \qquad (6)
$$

where $\upsilon=[\upsilon_1^T,\upsilon_2^T]^T$ represents the linear and angular velocities computed in the body fixed coordinate frame, $\tau_{RB}=[\tau_1^T,\tau_2^T]^T$ is the vector of forces and moments acting on the body, $\mathbf{M}_{RB}$ is the rigid body inertia matrix of the form

$$
\mathbf{M}_{RB}=\begin{bmatrix} m\mathbf{I}_{3\times3} & -mS(r_G) \\ mS(r_G) & \mathbf{I}_0 \end{bmatrix}=\begin{bmatrix}
m & 0 & 0 & 0 & mz_G & -my_G \\
0 & m & 0 & -mz_G & 0 & mx_G \\
0 & 0 & m & my_G & -mx_G & 0 \\
0 & -mz_G & my_G & I_x & -I_{xy} & -I_{xz} \\
mz_G & 0 & -mx_G & -I_{yx} & I_y & -I_{yz} \\
-my_G & mx_G & 0 & -I_{zx} & -I_{zy} & I_z
\end{bmatrix} \qquad (7)
$$

here $\mathbf{I}_0$ is the inertia tensor with respect to the origin of the body-fixed coordinate frame and $S(\cdot)$ is the skew-symmetric operator. For example let $\vec{A}=\begin{bmatrix} a_1 & a_2 & a_3 \end{bmatrix}^T$, then

$$S\left(\vec{A}\right)=\begin{bmatrix} 0 & -a_3 & a_2 \\ a_3 & 0 & -a_1 \\ -a_2 & a_1 & 0 \end{bmatrix} \quad \text{and} \quad S\left(\vec{A}\right)+S\left(\vec{A}\right)^T=[0]_{3\times 3}$$

Finally, $\mathbf{C}_{RB}(\upsilon)$ is the Coriolis or centripetal matrix

$$\mathbf{C}_{RB}(\upsilon)=\begin{bmatrix} 0 & 0 & 0 \\ 0 & 0 & 0 \\ 0 & 0 & 0 \\ -m(y_G q+z_G r) & m(x_G q-w) & m(x_G r+v) \\ m(y_G p+w) & -m(z_G r+x_G p) & m(y_G r-u) \\ m(z_G p-v) & m(z_G\, q+u) & -m(x_G p+y_G q) \end{bmatrix} \cdots$$

$$\cdots \begin{bmatrix} m(y_G q+z_G r) & -m(x_G q-w) & -m(x_G r+v) \\ -m(y_G p+w) & m(z_G r+x_G p) & -m(y_G r-u) \\ -m(z_G p-v) & -m(z_G\, q+u) & m(x_G p+y_G q) \\ 0 & -I_{yz} q-I_{xz} p+I_z r & I_{yz} r+I_{xy} p-I_y q \\ I_{yz} q+I_{xz} p-I_z r & 0 & -I_{xz} r-I_{xy} q+I_x p \\ -I_{yz} r-I_{zy} p+I_y q & I_{xz} r+I_{xy} q-I_x p & 0 \end{bmatrix} \quad (8)$$

B. GENERIC HYDRODYNAMIC MODEL

For a submerged rigid body the forces and moments acting upon it can be modeled in the form

$$\tau_{RB}=\tau_H+\tau_E+\tau \,. \quad (9)$$

τ_E is the vector of environmental forces and moments (disturbances) induced on the rigid body, τ is the propulsive forces and moments induced by the actuators (thrusters) on the body. τ_H is the hydrodynamic forces and moments, and is typically modeled as

$$\tau_H=-\mathbf{M}_A\dot{\upsilon}-\mathbf{C}_A(\upsilon)\upsilon-\mathbf{D}(\upsilon)\upsilon-g(\eta) \,. \quad (10)$$

$\mathbf{M}_A$ is the added inertia matrix, $\mathbf{C}_A(\upsilon)$ is the hydrodynamic Coriolis and centripetal forces matrix, and $\mathbf{D}(\upsilon)$ is the potential damping matrix . $g(\eta)$ is the restoring forces and moments, which depend on the pose of the body, η, where

$$\eta=[\eta_1^T,\eta_2^T]^T; \qquad \eta_1=[x,y,z]^T; \qquad \eta_2=[\phi,\theta,\psi]^T$$

The matrix $\mathbf{M}_A$ has the following generic form

$$\mathbf{M}_A = \begin{bmatrix} \mathbf{A}_{11} & \mathbf{A}_{21} \\ \mathbf{A}_{12} & \mathbf{A}_{22} \end{bmatrix} = \begin{bmatrix} X_{\dot{u}} & X_{\dot{v}} & X_{\dot{w}} & X_{\dot{p}} & X_{\dot{q}} & X_{\dot{r}} \\ Y_{\dot{u}} & Y_{\dot{v}} & Y_{\dot{w}} & Y_{\dot{p}} & Y_{\dot{q}} & Y_{\dot{r}} \\ Z_{\dot{u}} & Z_{\dot{v}} & Z_{\dot{w}} & Z_{\dot{p}} & Z_{\dot{q}} & Z_{\dot{r}} \\ K_{\dot{u}} & K_{\dot{v}} & K_{\dot{w}} & K_{\dot{p}} & K_{\dot{q}} & K_{\dot{r}} \\ M_{\dot{u}} & M_{\dot{v}} & M_{\dot{w}} & M_{\dot{p}} & M_{\dot{q}} & M_{\dot{r}} \\ N_{\dot{u}} & N_{\dot{v}} & N_{\dot{w}} & N_{\dot{p}} & N_{\dot{q}} & N_{\dot{r}} \end{bmatrix}. \tag{11}$$

$\mathbf{M}_A$ is always a positive definite matrix for submerged bodies. The elements of this matrix can be thought as the partial derivative of the propulsion forces and moments with respect to acceleration over the axes of the body-fixed coordinate frame, for example

$$X_{\dot{w}} \triangleq \frac{\partial X}{\partial \dot{w}}. \tag{12}$$

In simpler terms, represents the added mass along the *x*-axis due to acceleration along the *z*-axis of the body frame, due to the volume of fluid that has to displace.

The elements of $\mathbf{M}_A$ are conveniently grouped, where $\mathbf{A}_{11}$ and $\mathbf{A}_{22}$ contain elements that involve translation added mass and rotation added inertia respectively, whereas elements of $\mathbf{A}_{12}$ and $\mathbf{A}_{21}$ involve added inertia and added mass respectively, due to coupled motion.

$\mathbf{C}_A(\upsilon)$ is an skew symmetric matrix, and it represents the added Coriolis and centripetal terms.

$$\mathbf{C}_A(\upsilon) = \begin{bmatrix} 0_{3\times 3} & -S(\mathbf{A}_{11}\upsilon_1 + \mathbf{A}_{12}\upsilon_2) \\ -S(\mathbf{A}_{11}\upsilon_1 + \mathbf{A}_{12}\upsilon_2) & -S(\mathbf{A}_{21}\upsilon_1 + \mathbf{A}_{22}\upsilon_2) \end{bmatrix}. \tag{13}$$

Substituting the values of equations (11) into equation (13), we obtain

$$\mathbf{C}_A(\upsilon) = \begin{bmatrix} 0 & 0 & 0 & 0 & -a_3 & a_2 \\ 0 & 0 & 0 & a_3 & 0 & -a_1 \\ 0 & 0 & 0 & -a_2 & a_1 & 0 \\ 0 & -a_3 & a_2 & 0 & -b_3 & b_2 \\ a_3 & 0 & -a_1 & b_3 & 0 & -b_1 \\ -a_2 & a_1 & 0 & -b_2 & b_1 & 0 \end{bmatrix}. \tag{14}$$

where

$$
\begin{aligned}
a_1 &= X_{\dot{u}}u + X_{\dot{v}}v + X_{\dot{w}}w + X_{\dot{p}}p + X_{\dot{q}}q + X_{\dot{r}}r \\
a_2 &= X_{\dot{v}}u + Y_{\dot{v}}v + Y_{\dot{w}}w + Y_{\dot{p}}p + Y_{\dot{q}}q + Y_{\dot{r}}r \\
a_3 &= X_{\dot{w}}u + Y_{\dot{w}}v + Z_{\dot{w}}w + Z_{\dot{p}}p + Z_{\dot{q}}q + Z_{\dot{r}}r \\
b_1 &= X_{\dot{p}}u + Y_{\dot{p}}v + Z_{\dot{p}}w + K_{\dot{p}}p + K_{\dot{q}}q + K_{\dot{r}}r \\
b_2 &= X_{\dot{q}}u + Y_{\dot{q}}v + Z_{\dot{q}}w + K_{\dot{q}}p + M_{\dot{q}}q + M_{\dot{r}}r \\
b_3 &= X_{\dot{r}}u + Y_{\dot{r}}v + Z_{\dot{r}}w + K_{\dot{r}}p + M_{\dot{r}}q + N_{\dot{r}}r
\end{aligned}
\quad . \tag{15}
$$

The matrix $\mathbf{D}(\upsilon)$ models the hydrodynamic damping of the body. It is generally composed of the following elements

$$
\mathbf{D}(\upsilon) \triangleq \mathbf{D}_P(\upsilon) + \mathbf{D}_S(\upsilon) + \mathbf{D}_W(\upsilon) + \mathbf{D}_M(\upsilon) \quad . \tag{16}
$$

$\mathbf{D}_P(\upsilon)$ represents the radiation-induced damping due to forced body oscillations; $\mathbf{D}_S(\upsilon)$ represents the linear skin friction due to laminar boundary layers and quadratic skin friction due to turbulent boundary layers; $\mathbf{D}_W(\upsilon)$ represents the wave drift damping, and $\mathbf{D}_M(\upsilon)$ represents the damping due to vortex shielding. This equation can be simplified for underwater vehicles, and this simplification will be mentioned in the following section of this chapter.

The vector $g(\eta)$ is the vector of restoring forces and moments

$$
g(\eta) = \begin{bmatrix}
(W-B)\sin\theta \\
-(W-B)\cos\theta\sin\phi \\
-(W-B)\cos\theta\cos\phi \\
-(y_G W - y_B B)\cos\theta\sin\phi + (z_G W - z_B B)\cos\theta\sin\phi \\
(z_G W - z_B B)\sin\theta + (x_G W - x_B B)\cos\theta\cos\phi \\
-(x_G W - x_B B)\cos\theta\sin\phi - (y_G W - y_B B)\sin\theta
\end{bmatrix} \tag{17}
$$

where B represents the buoyancy force that the fluid projects over the submerged body, and W is the weight of the body in air. $r_B \triangleq [x_B \quad y_B \quad z_B]^T$ is the vector that represents the position of the center of buoyancy, and $r_G \triangleq [x_G \quad y_G \quad z_G]^T$ represents the position of the center of gravity relative to the body-fixed frame.

Finally, substituting these definitions into equations (6) and (9), the following expression is obtained

$$\mathbf{M}\dot{\upsilon} + \mathbf{C}(\upsilon)\upsilon + \mathbf{D}(\upsilon)\upsilon + g(\eta) = \tau_E + \tau \tag{18}$$

where in this expression $\mathbf{M} \triangleq \mathbf{M}_{RB} + \mathbf{M}_A$ and $\mathbf{C}(\upsilon) \triangleq \mathbf{C}_{RB}(\upsilon) + \mathbf{C}_A(\upsilon)$.

C. ASSUMPTIONS AND SIMPLIFICATIONS

The generic equations of motion derived in the previous section can be simplified by using a clever choice of coordinate systems and assumptions. According to Fossen [1],

> The simplest form of the equations of motion is obtained when the body axes coincide with the principal axes of inertia. This implies that $\mathbf{I}_C = \text{diag}\{I_{x_C}, I_{y_C}, I_{z_C}\}$.

For this research, it will also be assumed that the x and y components of both the center of gravity and the center of buoyancy coincide with the origin of the body-fixed coordinate frame [4], therefore

$$r_G = [0, 0, z_G]^T; \qquad r_B = [0, 0, z_B]^T \tag{19}$$

Neutral buoyancy is also assumed, simplifying the restoring forces and moments $g(\eta)$ to

$$g(\eta) = \begin{bmatrix} 0 \\ 0 \\ 0 \\ -F_{BK} \\ F_{BM} \\ 0 \end{bmatrix} \tag{20}$$

where $F_{BK} = B(z_G - z_B)\cos\theta\sin\phi$ and $F_{BM} = B(z_G - z_B)\sin\theta$, the rigid body inertia matrix $\mathbf{M}_{RB}$ to

$$\mathbf{M}_{RB} = \begin{bmatrix} m & 0 & 0 & 0 & mz_G & 0 \\ 0 & m & 0 & -mz_G & 0 & 0 \\ 0 & 0 & m & 0 & 0 & 0 \\ 0 & -mz_G & 0 & I_x & 0 & 0 \\ mz_G & 0 & 0 & 0 & I_y & 0 \\ 0 & 0 & 0 & 0 & 0 & I_z \end{bmatrix} \tag{21}$$

and the Coriolis and centripetal rigid body matrix to

$$\mathbf{C}_{RB} = \begin{bmatrix} 0 & 0 & 0 & mz_G r & mw & -mv \\ 0 & 0 & 0 & -mw & mz_G r & mu \\ 0 & 0 & 0 & -m(z_G p - v) & -m(z_G q + u) & 0 \\ -mz_G r & mw & m(z_G p - v) & 0 & I_z r & -I_y q \\ -mw & -mz_G r & m(z_G q + u) & -I_z r & 0 & I_x p \\ mv & -mu & 0 & I_y q & -I_x p & 0 \end{bmatrix} \tag{22}$$

Moreover, assuming that the vehicle has three planes of symmetry that coincide with the body-fixed frame axes and operates performing non-coupled motion simplifies the added mass and inertia matrix to

$$\mathbf{M}_A = -\text{diag}\{X_{\dot{u}}, Y_{\dot{v}}, Z_{\dot{w}}, K_{\dot{p}}, M_{\dot{q}}, N_{\dot{r}}\} \tag{23}$$

Thus, the added Coriolis and centripetal terms become

$$\mathbf{C}_A(\upsilon) = \begin{bmatrix} 0 & 0 & 0 & 0 & -Z_{\dot{w}} w & Y_{\dot{v}} v \\ 0 & 0 & 0 & Z_{\dot{w}} w & 0 & -X_{\dot{u}} u \\ 0 & 0 & 0 & -Y_{\dot{v}} v & Z_{\dot{w}} w & 0 \\ 0 & -Z_{\dot{w}} w & Y_{\dot{v}} v & 0 & -N_{\dot{r}} r & M_{\dot{q}} q \\ Z_{\dot{w}} w & 0 & -X_{\dot{u}} u & N_{\dot{r}} r & 0 & -K_{\dot{p}} p \\ -Y_{\dot{v}} v & Z_{\dot{w}} w & 0 & -M_{\dot{q}} q & K_{\dot{p}} p & 0 \end{bmatrix}. \tag{24}$$

Furthermore, the latter simplification, for underwater vehicles, simplifies the matrix of hydrodynamic damping to

$$\begin{aligned} \mathbf{D}(\upsilon) = & -\text{diag}\{X_u, Y_v, Z_w, K_p, M_q, N_r\} \ldots \\ & \ldots - \text{diag}\{X_{u|u|}|u|, Y_{v|v|}|v|, Z_{w|w|}|w|, K_{p|p|}|p|, M_{q|q|}|q|, N_{r|r|}|r|\} \end{aligned} \tag{25}$$

These assumptions yield to the following simplified equations of motion for the six degrees of freedom:

$$
\begin{aligned}
X_{prop} &= (m - X_{\dot{u}})\dot{u} - (m - Y_{\dot{v}})vr + (m - Z_{\dot{w}})wq - X_u u - X_{u|u|} u|u| \\
Y_{prop} &= (m - Y_{\dot{v}})\dot{v} - (m - Z_{\dot{w}})wp + (m - X_{\dot{u}})ur - Y_v v - Y_{v|v|} v|v| \\
Z_{prop} &= (m - Z_{\dot{w}})\dot{w} - (m - X_{\dot{u}})uq + (m - Y_{\dot{v}})vp - Z_w w - Z_{w|w|} w|w| \\
K_{prop} &= (I_x - K_{\dot{p}})\dot{p} + (Y_{\dot{v}} - Z_{\dot{w}})wv + (I_z - I_y + N_{\dot{r}} + M_{\dot{q}})rq \\
&\quad -K_p\, p - K_{p|p|}\, p|p| - F_{BK} \\
M_{prop} &= (I_y - M_{\dot{q}})\dot{q} + (Z_{\dot{w}} - X_{\dot{u}})uw + (I_y - I_x + N_{\dot{r}} - K_{\dot{p}})rp \\
&\quad -M_q\, q - M_{q|q|}\, q|q| + F_{BM} \\
N_{prop} &= (I_z - N_{\dot{r}})\dot{r} + (X_{\dot{u}} - Y_{\dot{v}})uv + (I_y - I_x + K_{\dot{p}} - M_{\dot{q}})rp \\
&\quad -N_r\, r - N_{r|r|}\, r|r|
\end{aligned}
\tag{26}
$$

Although simplified, this version of the EOMs is still highly coupled and non-linear, making the experimental identification of hydrodynamic coefficients a challenging task. This will be further explored in Chapter V.

THIS PAGE INTENTIONALLY LEFT BLANK

III. SYSTEM IDENTIFICATION

As seen in the previous chapter, the simplified EOMs (26) still counts with several unknown coefficients. While some of these coefficients can be measured, like the mass and the moment of inertia, further explored in chapter IV, the rest must be obtained experimentally. This chapter presents the tool that would be used in this research to identify the unknown hydrodynamic parameters of the EOMs.

A. RECURSIVE LEAST SQUARE ESTIMATOR

Given an overdetermined linear system:

$$y(t) = \Phi(x(t))\Theta \tag{27}$$

where $\Phi(x(t))$ is a known, time dependent section (regressor) and Θ is an unknown, time invariant section (parameters), there is not a unique solution. Instead, a "closest" solution exists

$$\hat{y}(t) = \Phi(x(t))\hat{\Theta} \tag{28}$$

$\hat{\Theta}$ are the estimated parameters that assure that the loss function

$$V(\Theta, t) = \frac{1}{2}(y(t) - \hat{y}(t))^2 \tag{29}$$

is minimized. This can be found using the least squares technique [15, 18] and has the following solution

$$\hat{\Theta} = (\Phi^T \Phi)^{-1} \Phi^T y \ . \tag{30}$$

The matrix $\Phi^T\Phi$ is always positive semidefinite, ensuring that equation (29) has a minimum, and this minimum is unique. This solution is also known as the left pseudo-inverse.

It is convenient to use this solution when dealing with static systems, where all the information coming from the measurements is already available; but for dynamic systems, where new information becomes available at each time step, it is more convenient to use a different approach. An estimator can be generated by minimizing the cost function

$$J(\hat{\Theta}(t)) = \int_0^t (\hat{\Theta}^T(t)\Phi(x(\tau)) - y(\tau))^2 d\tau \tag{31}$$

with respect to $\hat{\Theta}(t)$. By computing the cost function gradient

$$\frac{1}{2}\frac{\partial J(\hat{\Theta}(t))}{\partial \hat{\Theta}} = \int_0^t \Phi(x(t))(\hat{\Theta}^T(t)\Phi(x(\tau)) - y(\tau))d\tau \tag{32}$$

and taking into consideration that the condition to minimize the cost function is

$$\frac{\partial J(\hat{\Theta}(t))}{\partial \hat{\Theta}} = 0 \quad , \tag{33}$$

this yields

$$\left[\int_0^t \Phi(x(t))\,\Phi^T(x(t))d\tau\right]\hat{\Theta}(t) = \int_0^t \Phi(x(t))y(\tau)d\tau \quad . \tag{34}$$

Moreover, assuming that the left hand side is invertible, the following expression is obtained

$$\hat{\Theta}(t) = \left[\int_0^t \Phi(x(t))\,\Phi^T(x(t))d\tau\right]^{-1}\int_0^t \Phi(x(t))y(\tau)d\tau \tag{35}$$

This solution of the least square problem allows to estimate the values of $\hat{\Theta}(t)$ as new information becomes available until it converges to true values (i.e., a recursive implementation). The downside is that constantly inversing the integral at every time step is computationally expensive. This issue can be overcome by introducing the adaptive gain Γ

$$\Gamma \triangleq \left[\int_0^t \Phi(x(t))\,\Phi^T(x(t))d\tau\right]^{-1} \tag{36}$$

and taking into consideration the following relationship

$$\frac{d}{dt}\left[\Gamma^{-1}(t)\right] = \frac{d}{dt}\left[\int_0^t \Phi(x(t))\,\Phi^T(x(t))d\tau\right] = \Phi(x(t))\,\Phi^T(x(t)) \quad . \tag{37}$$

Furthermore, by using the chain rule

$$\Gamma(t)\Gamma^{-1}(t) = I_{N\times N} \Rightarrow 0 = \frac{d}{dt}\left[\Gamma(t)\Gamma^{-1}(t)\right] = \dot{\Gamma}\Gamma^{-1} + \Gamma\dot{\Gamma}^{-1} \tag{38}$$

and combining equations (37) and (38), we obtain

$$\dot{\Gamma} = -\Gamma\dot{\Gamma}^{-1}\Gamma = -\Gamma\,\Phi\,\Phi^T\Gamma \quad . \tag{39}$$

This result allows the recursive computation of Γ as new information, given by $\Phi(x(t))$ becomes available. Additionally, differentiating equation (35)

$$\dot{\Gamma}^{-1}(t)\hat{\Theta}(t) + \Gamma^{-1}(t)\dot{\hat{\Theta}}(t) = \Phi(x(t))\, y(t) \tag{40}$$

and combining it with equation (37) yields

$$\dot{\hat{\Theta}} = \Gamma\Phi(y - \Phi^T\hat{\Theta}) \tag{41}$$

Equations (39) and (41) combined are known as the recursive version of the Least Squares Estimator (RLSE).

B. PARAMETER ESTIMATION FOR DYNAMIC SYSTEMS

In this work, it is required to perform system identification on a system of the form:

$$\begin{aligned} \dot{x} &= f_0(x,u) + f(x,u) \\ y &= Cx \end{aligned} \tag{42}$$

where $f_0(x,u)$ represents the known dynamics of the system and $f(x,u)$ the unknown dynamics. This latter part is written as the product of a known regressor $\Phi(x,\mathrm{u})$ and a matrix of unknown parameters Θ. One approach is to numerically differentiate the measurements to obtain $\dot{x}$ so as to use the methods developed in the previous section. However, differentiation of digital signals increases the amount of noise existing on the original data, leading to inaccurate information. Thus, it is desirable to instead convert the dynamic system to an equivalent static system [4] in order to apply the recursive method mentioned in the previous section.

Start by rewriting equation (42) as

$$\dot{x} + ax = ax + f_0(x,u) + \Phi(x,u)\Theta \tag{43}$$

and introducing a filtered version of the x, x_f

$$\dot{x}_f + ax_f = ax \quad . \tag{44}$$

Equation (44) is basically a low-pass filter, where a is the filtering constant. Let

$$z = x - x_f \qquad \rightarrow \qquad \dot{z} = \dot{x} - \dot{x}_f \quad . \tag{45}$$

Using equations (44) and (45), equation (43) can be written as

$$\dot{z} + az = f_0(x,u) + \Phi(x,u)\Theta \tag{46}$$

This first order differential equation has a unique solution

$$z(t) = e^{-at}z(0) + \int_0^t e^{-a(t-\tau)} f_0(x,u)d\tau + \int_0^t e^{-a(t-\tau)}\Phi(x,u)d\tau\,\Theta \tag{47}$$

Letting $\Phi_0 \triangleq \int_0^t e^{-a(t-\tau)} f_0(x,u)d\tau$ and $\Phi_f \triangleq \int_0^t e^{-a(t-\tau)}\Phi(x,u)d\tau$, and assuming that the initial conditions of the system are

$$x_f(0) = x(0) \quad \rightarrow \quad z(0) = 0$$

equation (47) can be simplified to

$$z(t) = \Phi_0 + \Phi_f\Theta \tag{48}$$

where Φ_0 and Φ_f are just filtered version of $f_0(x,u)$ and $\Phi(x,u)$, respectively. Furthermore, using (42) and (45), equation (48) can be rewritten as

$$y - Cx_f - C\Phi_0 = C\Phi_f\Theta \tag{49}$$

Finally, Φ_0 and Φ_f can also be computed recursively, since

$$\begin{aligned}\dot{\Phi}_0 &= -a\Phi_0 + f_0(x,u)\\ \dot{\Phi}_f &= -a\Phi_f + \Phi(x,u)\end{aligned}. \tag{50}$$

This equivalent static system allows setting a regressor to recursively estimate the vector of unknown parameters Θ. This has the advantage of not differentiating the measured velocities.

C. PERSISTENCE OF EXCITATION

Even for a non-excited system, parameters could be obtained using the methods shown above. These parameters would be found to be trivial and useless. The richness of the input signal is of great importance to ensure quality of the identified parameters.

From equation (30) we see that the matrix $\Phi^T\Phi$ is given by:

$$\Phi^T\Phi = \begin{bmatrix} \sum_{n+1}^{t} u^2(k-1) & \sum_{n+1}^{t} u(k-2)u(k-1) & \cdots & \sum_{n+1}^{t} u(k-n)u(k-1) \\ \sum_{n+1}^{t} u(k-1)u(k-2) & \sum_{n+1}^{t} u^2(k-2) & & \sum_{n+1}^{t} u(k-n)u(k-2) \\ \vdots & & \ddots & \\ \sum_{n+1}^{t} u(k-1)u(k-n) & & & \sum_{n+1}^{t} u^2(k-n) \end{bmatrix}, \quad (51)$$

where *u* are the input signals fed to the system, *k* is the total number of time steps, and *n* is the number of parameters of the system. This matrix needs to be full rank to be invertible. This is called an excitation condition [17]. For long data sets, the sums can be taken from 1 to *t*, obtaining

$$C_n = \lim_{t\to\infty} \frac{1}{t}\Phi^T\Phi = \begin{bmatrix} c(0) & c(1) & \cdots & c(n-1) \\ c(1) & c(0) & & c(n-2) \\ \vdots & & \ddots & \\ c(n-1) & c(n-2) & & c(0) \end{bmatrix}. \quad (52)$$

u is called *persistently exciting* (PE) if the matrix C_n is positive definite, in other words for any arbitrary vector a, $a^T C_n a > 0$.

D. IMPLEMENTATION AND SIMULATION RESULTS

In the pursuit of methodology verification, a simulation test was developed. Weiss [4] was able to identify the added mass and quadratic damping coefficients of the standard vLBV300 using a RLLS. These coefficients were used to generate a simulated velocity profile in each degree of freedom to corroborate that the RLSE approach used in this research converged to true values. Noise was added to the generated signal to improve the authenticity of the simulation and to legitimately verify the performance of the investigated regression. In addition to the hydrodynamic coefficients, additional characteristics of the system were needed to calculate the required parameters, such as the mass (for *surge*, *sway* and *heave*) and the moment of inertia with respect to the *z* axis (for *yaw*). This will be further explained in Section B of Chapter V. These parameters were also taken from Weiss report, where $m = 20.9\,kg$ and $I_Z = 0.90\,kg\,m^2$.

First, a non PE input signal, a step input, was used to excite the simulator. The convergence of the estimated parameters of the RLSE can be observed in Figure 6 and Figure 7 shows a comparison of the simulated velocity using the assumed parameters vs. a simulated velocity using the estimated parameters.

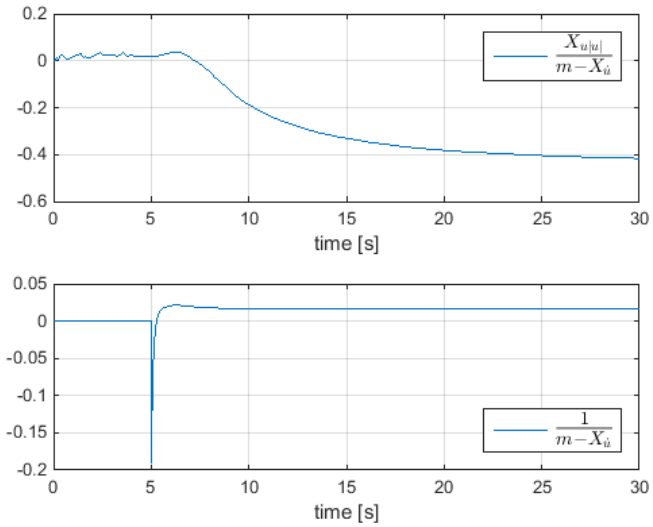

Figure 6. Convergence of parameters on the surge DOF during simulation with a non-PE input signal

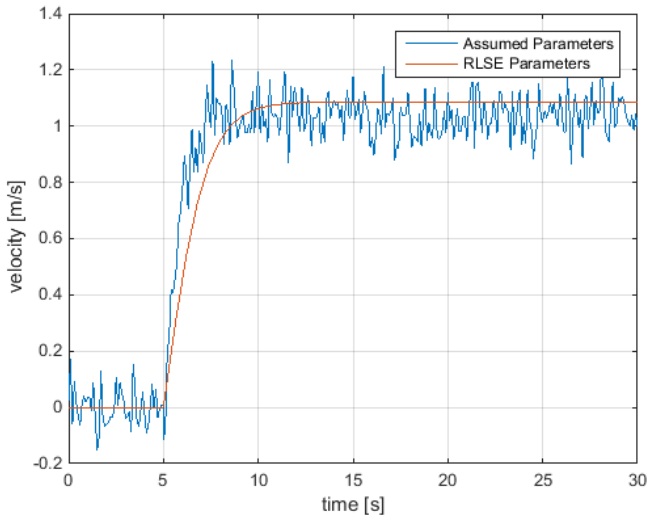

Figure 7. Generated velocity using assumed parameters vs. simulated velocity used estimated parameters with a non-PE input signal

The parameters converged and generated a fairly good velocity response, as seen in Figure 6 and Figure 7, respectively. However, comparing the estimated parameters with the assumed ones revealed a large error in most of the channels, as seen in Table 3. In other words, even though the parameters converged, they did not converge to the true values.

Table 3. Assumed hydrodynamic coefficients vs. coefficients obtained using RLSE using a non-PE input signal

	Assumed Value	Estimated Value	Units	Rel. Err. $(\Delta x / x)$
$X_{u\|u\|}$	-27.7411	-25.4321	kg/m	8.32 %
$X_{\dot{u}}$	-13.5778	-40.5778	kg	195.70 %
$Y_{v\|v\|}$	-50.6868	-38.7742	kg/m	23.50 %
$Y_{\dot{v}}$	-27.9347	-129.5184	kg	363.64 %

The same procedure was repeated using a series of varying step commands in an effort to persistently excite the system. Figure 8 and Figure 9 were generated using the estimated parameters for this case.

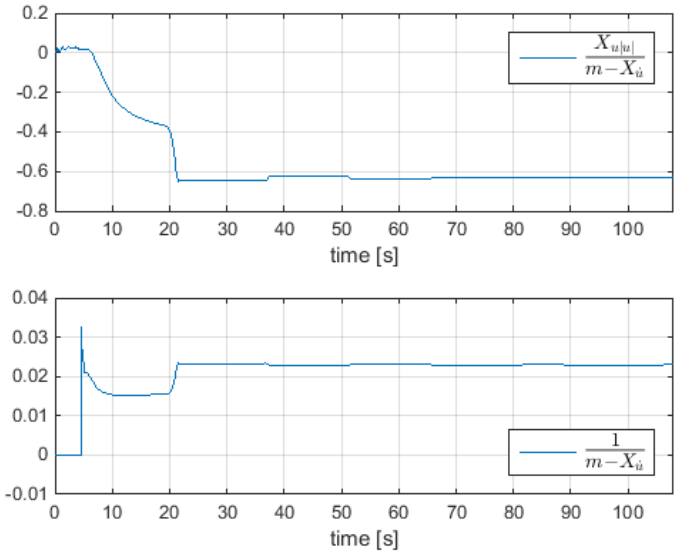

Figure 8. Convergence of parameters on the surge DOF during simulation

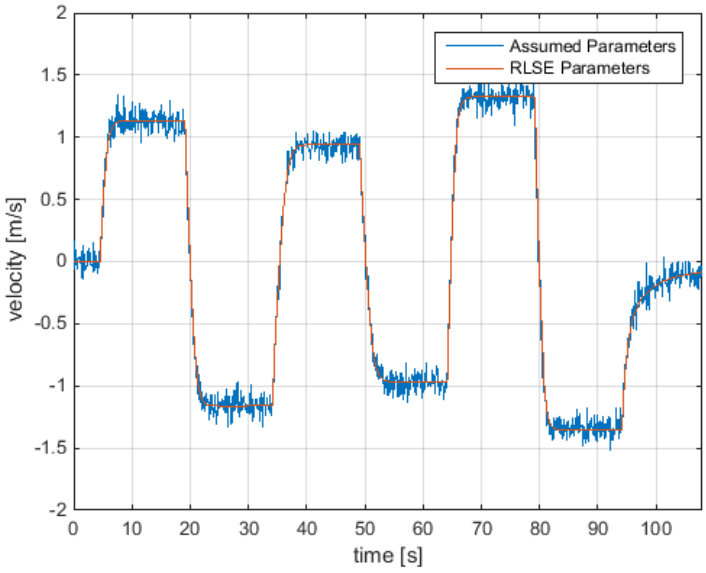

Figure 9. Generated velocity using assumed parameters vs. simulated velocity used estimated parameters

Figure 8 shows a fast convergence and a bounded stability at the steady state of the estimated parameters during the simulation of the velocity profile of the surge DOF. The simulation was carried out with the rest of the channels, and the results are

summarized in Table 4. The coefficients obtained by the RLSE are close to the assumed values, as reflected by the relative error.

Table 4. Assumed hydrodynamic coefficients vs. coefficients obtained using RLSE a PE input signal

	Assumed Value	Estimated Value	Units	Rel. Err. $(\Delta x / x)$
$X_{u\|u\|}$	-27.7411	-27.4633	kg/m	1.00 %
$X_{\dot{u}}$	-13.5778	-13.3967	kg	1.33 %
$Y_{v\|v\|}$	-50.6868	-50.3438	kg/m	0.68 %
$Y_{\dot{v}}$	-27.9347	-27.4153	kg	1.86 %
$Z_{w\|w\|}$	-64.5970	-63.0540	kg/m	2.39 %
$Z_{\dot{w}}$	-46.3258	-45.6039	kg	1.56 %
$N_{r\|r\|}$	-2.1709	-2.1709	$\mathrm{kg\,m^2/rad^2}$	0.25 %
$N_{\dot{r}}$	-3.1023	-3.0935	$\mathrm{kg\,m^2/rad}$	0.30 %

THIS PAGE INTENTIONALLY LEFT BLANK

IV. QUADRIFILAR PENDULUM

In Section A of Chapter II, the dynamics of a rigid body were derived with respect to some of the properties of the body, such as the mass (m) and the inertia tensor ($\mathbf{I}$). While the mass of an object is a property fairly easy to identify with the right instrumentation, this is not the case for the inertia tensor.

A. THEORY

The inertia tensor is a matrix composed by the moments of inertia (main diagonal values) and the products of inertia (off diagonal) of the body about a chosen coordinate frame (0). From Fossen [1]:

$$\mathbf{I}_0 \triangleq \begin{bmatrix} I_x & -I_{xy} & -I_{xz} \\ -I_{yx} & I_y & -I_{xy} \\ -I_{zx} & -I_{zy} & I_z \end{bmatrix}; \qquad \mathbf{I}_0 = \mathbf{I}_0^{\,T} \tag{53}$$

All the individual elements of the inertia matrix can be identified performing the following computation:

$$\begin{aligned} I_x &= \int_V (y^2 + z^2)\rho dV; & I_{xy} &= \int_V xy\rho dV \\ I_y &= \int_V (x^2 + z^2)\rho dV; & I_{xz} &= \int_V xz\rho dV \\ I_z &= \int_V (x^2 + y^2)\rho dV; & I_{yz} &= \int_V yz\rho dV \end{aligned}$$

where ρ is the density of the body and V is the volume.

Computing these parameters is an easy task for simple geometrically shaped bodies, but as the shape grows in complexity, so does the difficulty of this calculation. Furthermore, engineering structures are usually composed of several different materials, each with a density of its own.

CAD models are one way to overcome this challenge, but require having access to the software and being skilled enough to draw complex models. In addition, individual components of the body might be more complex than the way they are modeled using this software, leading to inaccuracies on the result. Finally, the objects for which these

properties must be determined in this research undergo configuration changes frequently, making the CAD modeling approach even less applicable.

Several techniques exist for the experimental determination of the moments of inertia [8], including multi-filar pendulums, as used in this research. Genta [7] uses a linearization and the Lagrange approach to calculate the natural frequency (λ) of a multi-filar pendulum in the θ degree of freedom (torsion).

$$\lambda_\theta = \sqrt{\frac{m_{eq} g R_1 R_2}{I_{eq} h}} \tag{54}$$

where m_{eq} is the combined mass of the object, tray and wires, g is the gravity and R_1 and R_2 are the radii of the circles that circumscribe the wire supports in the ceiling and the tray respectively. The period between oscillations is computed as:

$$T = \frac{2\pi}{\lambda} \tag{55}$$

Combining equations (54) and (55), yields

$$I_{eq} = \frac{m_{eq} g R_1 R_2}{4\pi^2 h} T^2 \quad . \tag{56}$$

Hence, the moment of inertia can be calculated by measuring the period of the oscillations. Furthermore, the moment of inertia of an object, I_O placed on top of the pendulum can be calculated by subtracting the moment of inertia of the pendulum, I_P, from the equivalent moment of inertia. In other words

$$I_O = I_{eq} - I_P \quad . \tag{57}$$

This holds true as long as the horizontal displacement of the pendulum is small enough to be considered negligible.

B. EXPERIMENTAL SETUP

A quadrifilar pendulum consists of a platform or a tray suspended in the air by four wires attached to the celling, as seen in Figure 10.

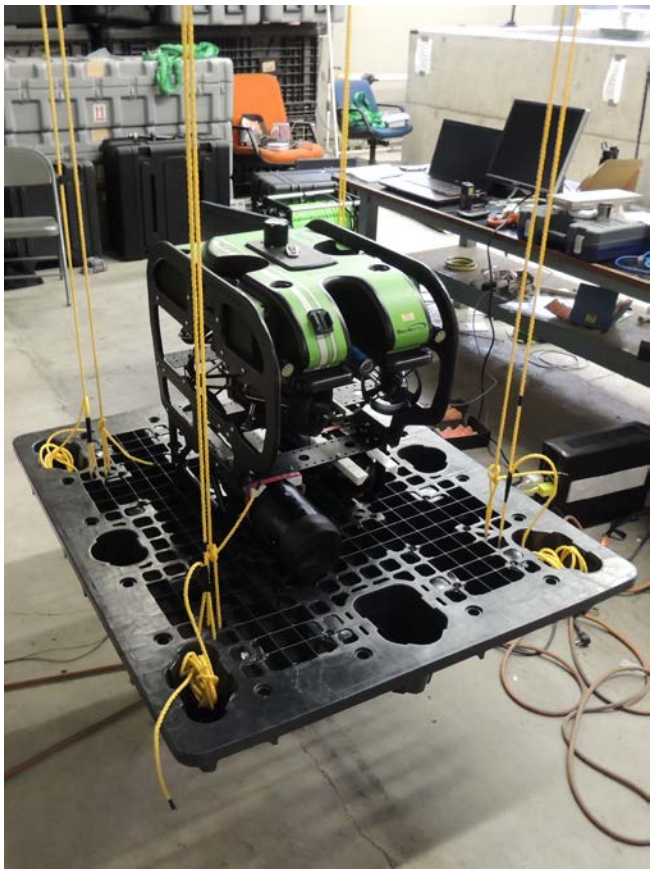

Figure 10. Quadrifilar pendulum during trials with the THAUS AUV.

For this setup, $R_1 = R_2 = 0.47\,\text{m}$, the weight of the tray $m_T = 9.8\,\text{kg}$ and the length of the lines $h = 4.23\,\text{m}$. A small initial excitation was induced on the platform to generate oscillations. The amount of time for 20 complete oscillations was measured in order to reduce the measurement error. Using this method, the moment of inertia of the pendulum was found, $I_P = 2.1970\,\text{kg}\,\text{m}^2$. To verify the validity of this experiment, the procedure was repeated with an aluminum tube on top of the pendulum, since its moments of inertia were easy to calculate. The equivalent moment of inertia was calculated as $I_{eq} = 2.8590\,\text{kg}\,\text{m}^2$, and the resulting moment of inertia of the aluminum tube was calculated as $I_O = 0.6620\,\text{kg}\,\text{m}^2$.

The solution of the moment of inertia of a hollow cylinder is

$$I_y = I_z = m\left(\frac{L^2}{12} + \frac{R^2 + r^2}{4}\right) \tag{58}$$

where R and r are the outer and inner diameter respectively, and L is the length of the cylinder. The properties of the aluminum tube used for this experiment are listed in Table 5.

Table 5. Properties and dimensions of the aluminum tube used for verification.

Parameter	Value	Units
m	2.3800	kg
L	1.8200	m
R	0.0254	m
r	0.0219	m

The calculated moment of inertia of the tube using equation (58) was $I_y = I_z = 0.6576\,\text{kg}\,\text{m}^2$

The moment of inertia calculated using the pendulum had a difference of 0.67% with the true moment of inertia of the body.

C. EXPERIMENTAL RESULTS

The same procedure was carried out with the THAUS AUV and REMUS AUV to capture the moment of inertia about each plane about their center of gravity. Prior to this test, the vehicles were weighted to identify their mass. The results are shown in Table 6.

Table 6. Mass properties of the vehicles

Vehicle	Mass	Units
THAUS	38.10	kg
REMUS	36.20	Kg

In Section C of Chapter II it was assumed that the body planes of symmetry coincide with the axes of the body-fixed frame. This assumption allows neglecting the

off-diagonal coefficients of the inertia tensor. The results are listed in Table 7 and Table 8, respectively.

Table 7. Calculated moment of inertia of the THAUS AUV

Parameter	Value	Units
I_x	1.7428	$\mathrm{kg\,m^2}$
I_y	2.2278	$\mathrm{kg\,m^2}$
I_z	1.4046	$\mathrm{kg\,m^2}$

Table 8. Calculated moment of inertia of the REMUS 100 ROV

Parameter	Value	Units
I_x	0.2777	$\mathrm{kg\,m^2}$
I_y	5.4133	$\mathrm{kg\,m^2}$
I_z	5.4133	$\mathrm{kg\,m^2}$

THIS PAGE INTENTIONALLY LEFT BLANK

V. SINGLE CHANNEL EXCITATION

Hovering underwater vehicles, like the THAUS AUV, have the advantage of being able to perform uncoupled motion on several degrees of freedom using one or more thrusters. This can be used to estimate the hydrodynamic coefficients corresponding to the channels that are possible to excite individually. This chapter explains how the system identification techniques proposed in Chapter III can be used in order to do so.

A. PREVIOUS WORK AT NPS

Weiss's [4] work set the foundations for the present research. In his work, an accurate model of the thrust generated by the propellers of the THAUS AUV was identified:

$$Thrust = 0.006736\ PWM^2 - 0.03366\ PWM + 0.0684\,. \tag{59}$$

This model is used extensively in the development of this chapter.

Several identification techniques were tested in order to perform real-time identification of the hydrodynamic coefficients of the equations of motion of the SeaBotix vLBV300. A Gradient Estimator (GE), Neural Network (NN), Bayesian filtering and Recursive Linear Least Squares (RLLS) estimation were studied, concluding that the GE and Bayesian filtering were not suitable or not applicable for this identification task. A simple NN that was able to map the thruster force in the surge DOF was created for both the simulator and the vLBV300. Next, a more complicated NN was set to capture the input-output relations of four DOFs: *surge, sway, heave* and *yaw.* This last NN was not able to capture enough data to accomplish its objective due to limitations of the experimental setup. Finally the RLLS was proven capable to estimate the parameters of the regressor.

The VICON cameras system was used to track the motion of the vLBV300, having the advantage of accurate tracking measurements, but was restricted to a small testing space.

For the identification method explained in this chapter, data from the onboard INS was used to identify the hydrodynamic parameters. This is a more versatile method, allowing the test to be carried almost everywhere, but sacrificing the accuracy of the VICON system.

B. METHODOLOGY

In Section C of Chapter II a simplified version of the equations of motion for underwater vehicles was developed. This parameterized governing equation of the surge motion is shown below

$$\dot{u} = \frac{(m - Y_{\dot{v}})vr - (m - Z_{\dot{w}})wq + X_u u + X_{u|u|} u|u| + X_{prop}}{(m - X_{\dot{u}})} \quad . \tag{60}$$

It is observable that even a simplified version, as the one shown above, is still highly coupled, making the parameter identification task more difficult.

A method to get around this issue is exciting individual channels, assuring little or no excitation in the remaining possible motions, allowing the coupled parameters to be neglected. The result is an equation of the form

$$\dot{u} = \frac{X_u}{(m - X_{\dot{u}})} u + \frac{X_{u|u|}}{(m - X_{\dot{u}})} u|u| + \frac{1}{(m - X_{\dot{u}})} X_{prop} \tag{61}$$

This has the form of equation (27), $y(t) = \Phi(x(t))\Theta$ (if $\dot{u}$ can be measured directly or can be converted into an equivalent static system, as demonstrated in Section B of Chapter III), where

$$\Phi(t) = \begin{bmatrix} u & u|u| & X_{prop} \end{bmatrix} \quad \text{and} \quad \Theta = \begin{bmatrix} \frac{X_u}{(m - X_{\dot{u}})} \\ \frac{X_{u|u|}}{(m - X_{\dot{u}})} \\ \frac{1}{(m - X_{\dot{u}})} \end{bmatrix} \tag{62}$$

The vectored thruster design of the THAUS AUV allows this (62) to be possible in five degrees of freedom: *surge, sway, heave, roll* (limited) and *yaw.*

$$
\begin{aligned}
\dot{v} &= \frac{Y_v}{(m-Y_{\dot{v}})}v + \frac{Y_{v|v|}}{(m-Y_{\dot{v}})}v|v| + \frac{1}{(m-Y_{\dot{v}})}Y_{prop} \\
\dot{w} &= \frac{Z_w}{(m-Z_{\dot{w}})}w + \frac{Z_{w|w|}}{(m-Z_{\dot{w}})}w|w| + \frac{1}{(m-Z_{\dot{w}})}Z_{prop} \\
\dot{p} &= \frac{K_p}{(I_x-K_{\dot{p}})}p + \frac{K_{p|p|}}{(I_x-K_{\dot{p}})}p|p| + \frac{F_{BK}}{(I_x-K_{\dot{p}})} + \frac{1}{(I_x-K_{\dot{p}})}K_{prop} \\
\dot{r} &= \frac{N_r}{(I_z-N_{\dot{r}})}r + \frac{N_{r|r|}}{(I_z-N_{\dot{r}})}r|r| + \frac{1}{(I_z-N_{\dot{r}})}N_{prop}
\end{aligned}
\tag{63}
$$

Due to the thruster configuration of the platform, the *pitch* DOF cannot be directly excited, but if the *surge* and *heave* DOFs are excited simultaneously, it is also possible to excite *pitch* due to the coupled nature of the motion [4]. Assuming that the unknown parameters of the *surge* and *heave* DOFs have been fully identified and the coupled motion is being induced only in the pitch DOF, by analyzing equation (64)

$$
\begin{aligned}
\dot{u} &= \frac{-(m-Z_{\dot{w}})wq + X_u u + X_{u|u|}u|u| + X_{prop}}{m-X_{\dot{u}}} \\
\dot{w} &= \frac{(m-X_{\dot{u}})uq + Z_w w + Z_{w|w|}w|w| + X_{prop}}{m-Z_{\dot{w}}} \\
\dot{q} &= \frac{-(Z_{\dot{w}}-X_{\dot{u}})uw + M_q q + M_{q|q|}q|q| + F_{BM}}{I_y - M_{\dot{q}}}
\end{aligned}
\tag{64}
$$

a regressor can be set, in terms of equation (50), as:

$$
f_0 = \begin{bmatrix}
\dfrac{-(m-Z_{\dot{w}})wq + X_u u + X_{u|u|}u|u| + X_{prop}}{m-X_{\dot{u}}} \\
\dfrac{(m-X_{\dot{u}})uq + Z_w w + Z_{w|w|}w|w| + X_{prop}}{m-Z_{\dot{w}}} \\
0
\end{bmatrix}
$$

$$
\Phi = \begin{bmatrix}
0 & 0 & 0 \\
0 & 0 & 0 \\
q & q|q| & F_{BM} - (Z_{\dot{w}}-X_{\dot{u}})uv
\end{bmatrix}
\tag{65}
$$

$$
\Theta = \begin{bmatrix}
\dfrac{M_q}{(I_y-M_{\dot{q}})} & \dfrac{M_{q|q|}}{(I_y-M_{\dot{q}})} & \dfrac{1}{(I_y-M_{\dot{q}})}
\end{bmatrix}
$$

C. SINGLE CHANNEL EXCITATION APPLIED TO THE THAUS AUV

By recording the velocity of the vehicle in each of the individually excited channels using the estimated states processed by the onboard INS, it is possible to apply the procedure explained before on the THAUS vehicle in order to estimate the hydrodynamic coefficients.

Three different damping models were compared using the gathered data: linear damping, quadratic damping and linear and quadratic damping. The Root Mean Square Error (RMSE) was calculated for each model. Results of this comparison for the *surge* channel are shown in Table 9 and a graphical comparison between the measured velocity and the velocity calculated with the identified parameters are shown in Figure 11, Figure 12 and Figure 13.

Table 9. Comparison between damping models for surge

Damping Model	$X_{\dot{u}}$	X_u	$X_{u\|u\|}$	RMSE
Linear and Quadratic	-94.8422	-27.9253	-72.7159	0.0020
Linear	-100.7447	-61.5144	--	0.0101
Quadratic	-91.7507	--	-132.2426	0.0015

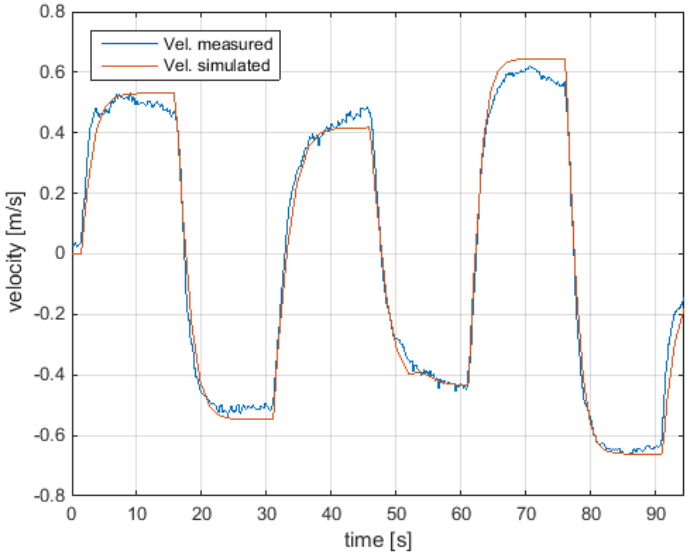

Figure 11. Measured velocity vs. calculated velocity using a linear and quadratic damping model

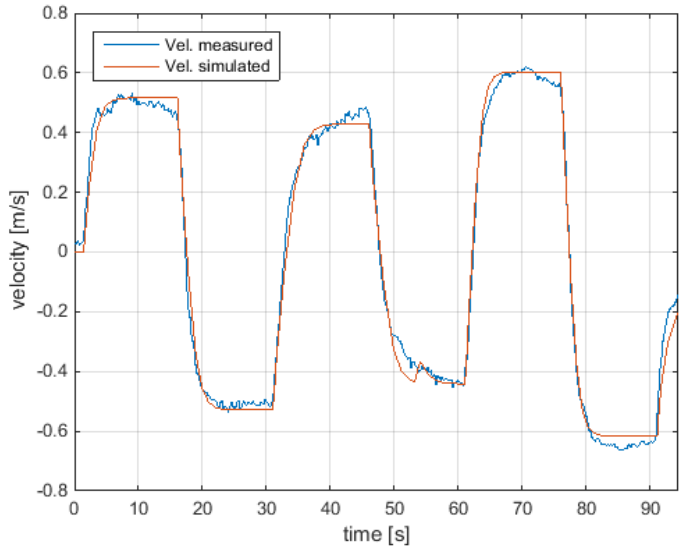

Figure 12. Measured velocity vs. calculated velocity using a quadratic damping model

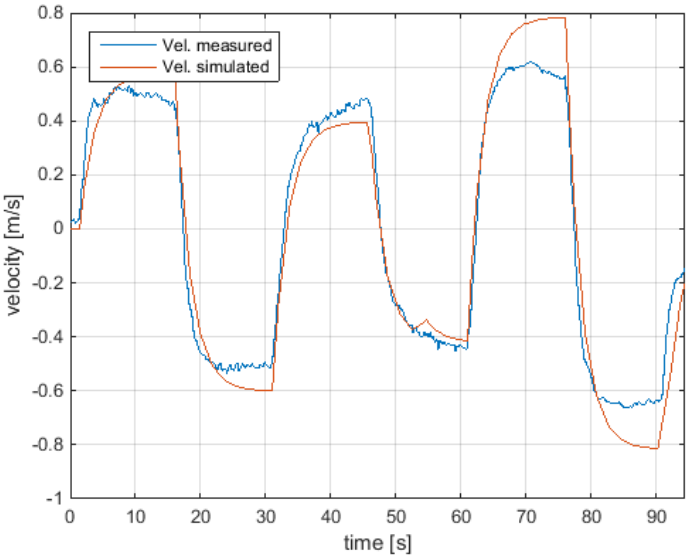

Figure 13. Measured velocity vs. calculated velocity using a linear damping model

In the case of the *surge* channel, the quadratic damping had the lowest RMSE. The same procedure was used in the rest of the degrees of freedom. The quadratic damping model was found to be the best fit for the *sway* and *yaw* channels as well. In the case of the *heave* channel, the linear quadratic model had the least RMSE. The estimated parameters for the four degrees of freedom are summarized in Table 10. The convergence of the estimated parameters using a quadratic damping model can be seen in Figure 14.

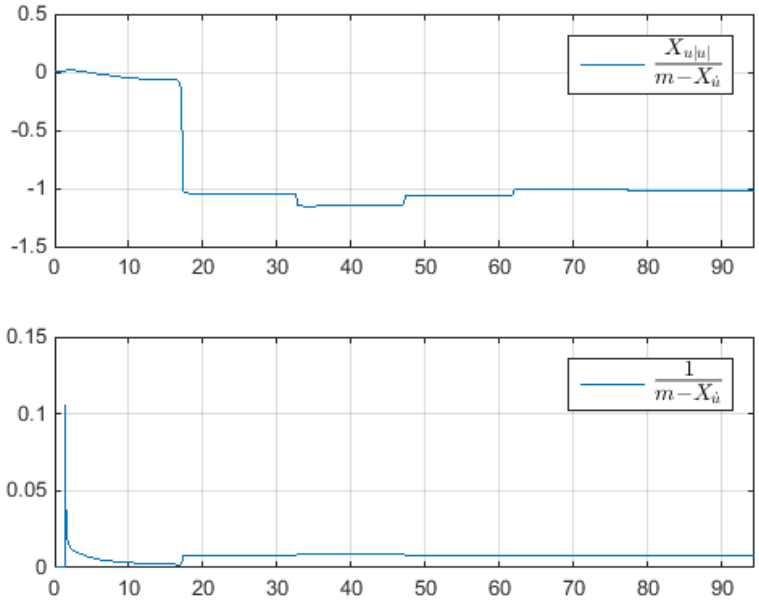

Figure 14. Convergence of parameters on the surge DOF using a quadratic damping model

Table 10. Hydrodynamic Coefficients of the THAUS AUV Using the Single Channel Excitation Technique

Parameter	Value	Units
$X_{u\|u\|}$	-132.2436	$\mathrm{kg/m}$
$X_{\dot{u}}$	-91.7507	kg
$Y_{v\|v\|}$	-357.8624	$\mathrm{kg/m}$
$Y_{\dot{v}}$	-205.0403	kg
Z_{w}	-85.9259	$\mathrm{kg/s}$
$Z_{\dot{w}}$	-194.9859	kg
$N_{r\|r\|}$	-5.8274	$\mathrm{kg\,m^2/rad^2}$
$N_{\dot{r}}$	-2.4765	$\mathrm{kg\,m^2/rad}$

THIS PAGE INTENTIONALLY LEFT BLANK

VI. FREE DECAY PENDULUM EXPERIMENT

As mentioned in Chapter V, hovering vehicles can excite several degrees of freedom individually. This is not possible for vehicles such as the REMUS 100 AUV, where *surge* is the only DOF that can be excited independently, while the rest of the degrees of freedom are coupled. However, with the developed free decay pendulum experimental setup it is possible to constrain the direction of the vehicle motion to a single degree of freedom, making it possible to estimate the associated hydrodynamic coefficients for the channels that cannot normally be excited.

A. EXPERIMENTAL SETUP

Eng *et al*. [6] first proposed the use of the free decay motion of the pendulum and a scale model of a vehicle to estimate the hydrodynamic coefficients of an underwater vehicle. Based on this work, an experimental setup was developed at NPS to apply the technique to NPS platforms for model learning. This experimental setup was designed (outside the scope of this research) and manufactured. The pendulum setup used in this research allows mounting THAUS and REMUS directly.

1. Hardware and Setup

The experimental setup consisted of two aluminum tubes joined with a pressure clamp and pinned to an aluminum base attached to the ceiling. This setup restricted the pendulum motion to a single degree of freedom. More details about the properties of this setup can be found in Table 11. A Pixhawk Px4 autopilot was attached to the pole of the pendulum, assuring that the device was aligned with the plane of motion of the pendulum in order to get measurements in the desired DOF (without coupling with the other DOFs). Data from its Inertial Measurements Unit (IMU) was used in order to measure the orientation and angular velocity of the pendulum during trials. Figure 15 showed the configuration of the pendulum used in this test.

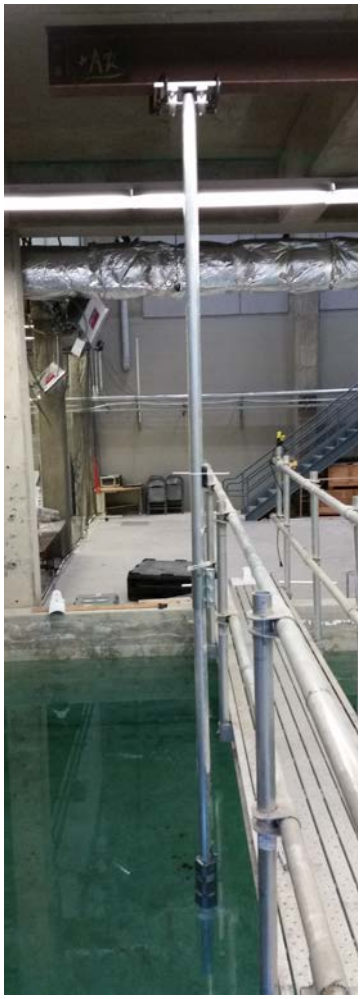

Figure 15. Pendulum Setup

Due to the low speed and damped oscillations achieved in the first trials, additional weight was added to the bottom tube of the pendulum for the sake of prolonging the oscillation of the pendulum on the heavily damped degrees of freedom of the vehicles.

This pendulum system was attached to the ceiling above the water test tank in the CAVR. Mounts for both the vLBV300 and the REMUS vehicles were 3D printed in order to attach the mentioned vehicles to the pendulum.

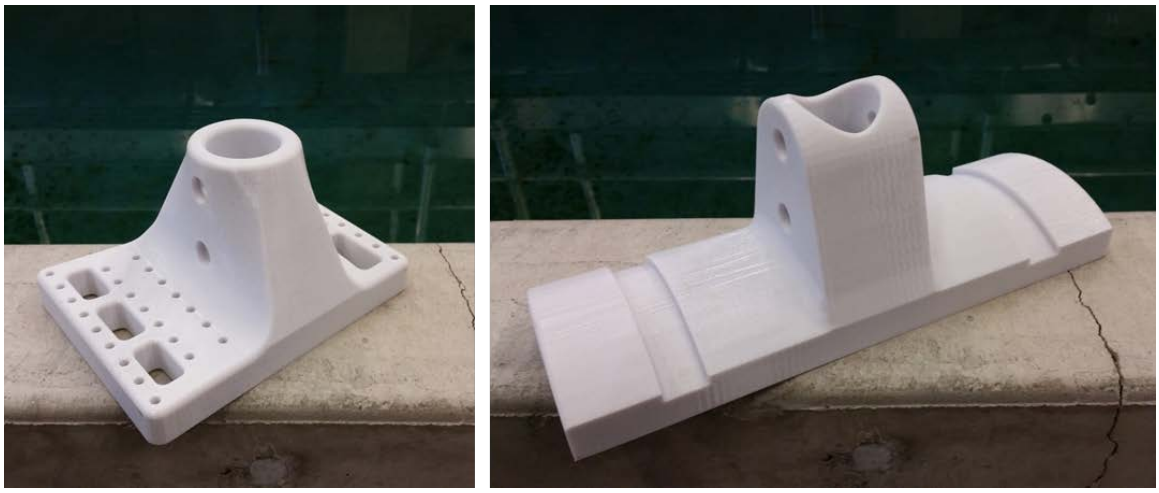

Figure 16. Mounts used to attach the THAUS AUV (left) and the REMUS AUV (right) to the pendulum.

2. Equations of Motion

The equations of motion corresponding to this set up were derived using a Newtonian approach; a free body diagram of the pendulum is shown in Figure 17.

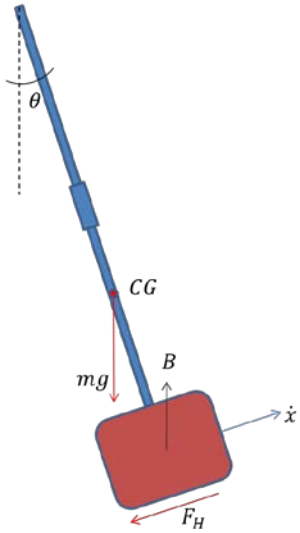

Figure 17. Free Body Diagram of the Pendulum

m is the combined mass of both the pendulum and the vehicle, B is the buoyancy force acting on the vehicle, and F_H is the sum of the hydrodynamic forces acting on the

vehicle due to its motion (i.e., due to damping and the added mass). Assuming that the excited degree of freedom of the vehicle mounted in the pendulum is *surge*, as seen in Figure 17, a Newtonian approach is used to model the dynamics of the pendulum:

$$m\dot{u} = B\sin\theta - Mg\sin\theta - F_H\,. \tag{66}$$

The hydrodynamic force acting on the vehicle is modeled as

$$F_H = -X_{\dot{u}}\dot{u} - X_u u - X_{u|u|}u|u|. \tag{67}$$

Keeping with the nomenclature used in Chapter II, $X_{\dot{u}}$, X_u and $X_{u|u|}$ is the added mass, linear damping and quadratic damping coefficients, respectively, corresponding to the *surge* DOF. Substituting (67) into (66) leads to

$$(m - X_{\dot{u}})\dot{u} = (B - Mg)\sin\theta + X_u u + X_{u|u|}u|u| \tag{68}$$

Moreover, the constrains of the pendulum only allow one degree of freedom motion, which is characterized in terms of the angle, θ, thus the following equivalences

$$u = L\dot{\theta};\ \dot{u} = L\ddot{\theta} \tag{69}$$

Substituting (69) into (68) and solving for the angular acceleration leads to

$$\ddot{\theta} = \frac{(B - Mg)}{(m - X_{\dot{u}})L}\sin\theta + \frac{X_u}{(m - X_{\dot{u}})}\dot{\theta} + \frac{X_{u|u|}L}{(m - X_{\dot{u}})}\dot{\theta}|\dot{\theta}|\ . \tag{70}$$

Equation (70) has a similar form to equation (27), which can be written in terms of the regressor and parameter matrix: $y(t) = \Phi(x(t))\Theta$,

$$\ddot{\theta} = \begin{bmatrix} \theta & \dot{\theta} & \dot{\theta}|\dot{\theta}| \end{bmatrix} \begin{bmatrix} \dfrac{(B - Mg)}{(m - X_{\dot{u}})L} \\ \dfrac{X_u}{(m - X_{\dot{u}})} \\ \dfrac{X_{u|u|}L}{(m - X_{\dot{u}})} \end{bmatrix}. \tag{71}$$

This allows us to use the same regression tools to identify the vector of unknown parameters presented in Chapter III and used in Chapter V.

3. Methodology

An initial angle of approximately 22 degrees was given to the pendulum at the start of the trials to induce the oscillations.

Table 11. Properties of the Components of the Pendulum

Parameter	Value	Units	Description
L	3.66	m	Length of the pendulum
m_p	5.93	kg	Mass of the pendulum
m_a	4.62	kg	Additional mass

The pendulum was excited first without any vehicle mounted, in order to calculate the added mass of the submerged portion of the pole. Table 11 summarizes the properties of the pendulum required for the calculation of the hydrodynamic coefficients. The result obtained was $\Theta_{\dot{\theta}} = -4.1996$ kg. This coefficient was later subtracted to obtain the added mass of the vehicles.

B. THAUS AUV RESULTS

The THAUS INS was used to gather the required orientation and angular velocity information. As described in Chapter V, three different models of damping were used and compared. The results of this comparison for the *surge* direction are shown in Table 12 and a graphical comparison between the calculated orientation and the measured orientation is shown in Figure 18, Figure 19 and Figure 20, for each of the respective damping models.

Table 12. Comparison between damping models for the *surge* DOF

Damping Model	$X_{\dot{u}}$	X_u	$X_{u\|u\|}$	RMSE
Linear and Quadratic	-87.0553	-45.7734	-0.6784	0.0612
Linear	-87.1206	-45.9694	--	0.0610
Quadratic	-110.6523	--	-3.0168	0.1894

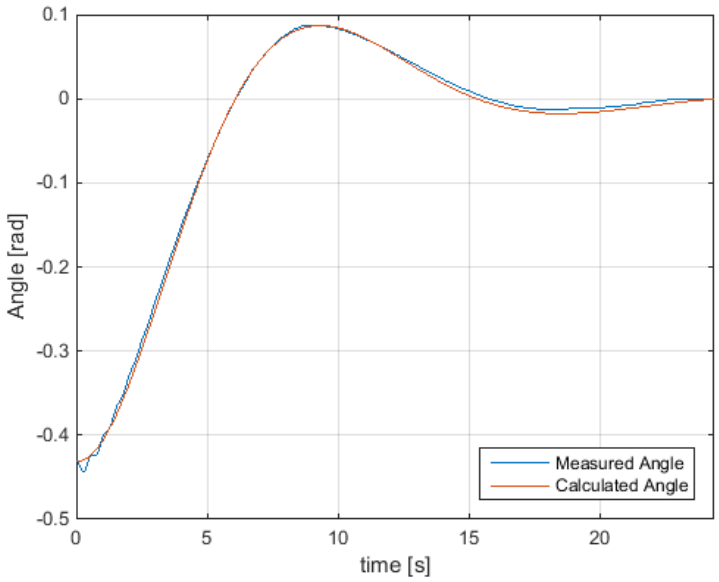

Figure 18. Measured vs. calculated orientation of the THAUS AUV with a linear and quadratic damping model in the *surge* DOF

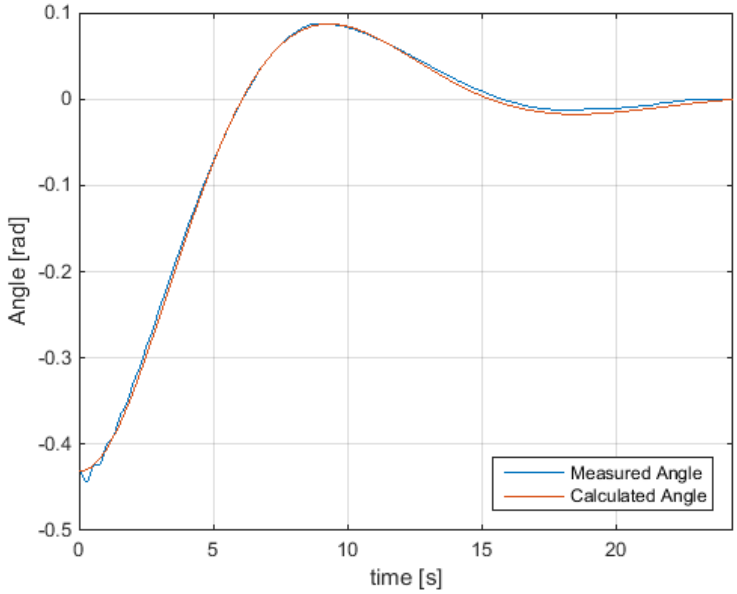

Figure 19. Measured vs. calculated orientation of the THAUS AUV with a linear damping model in the *surge* DOF

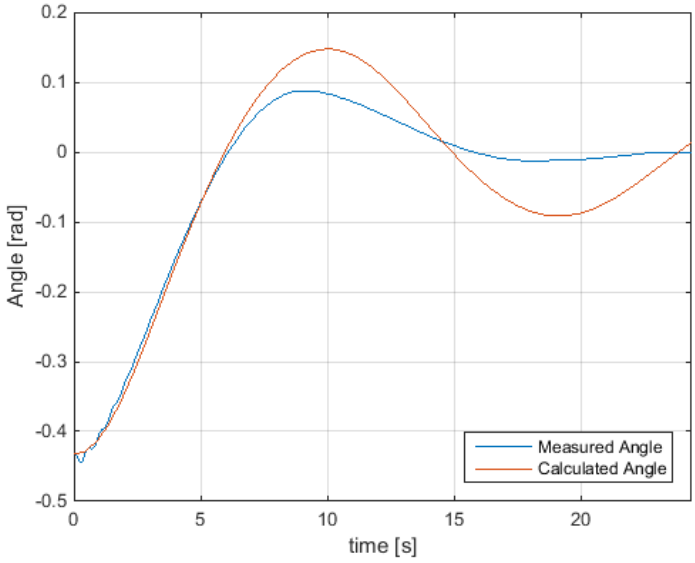

Figure 20. Measured vs. calculated orientation of the THAUS AUV with a quadratic damping model in the *surge* DOF

As seen in Table 12 even when modeled with linear and quadratic damping, the linear damping dominated over the quadratic due to the slow motion of the pendulum. Figure 21 shows the velocity of the THAUS AUV during this test, obtained by multiplying the measured angular velocity by the length of the pivot point to the center of mass of the vehicle. The maximum velocity registered was 0.3515 m/s.

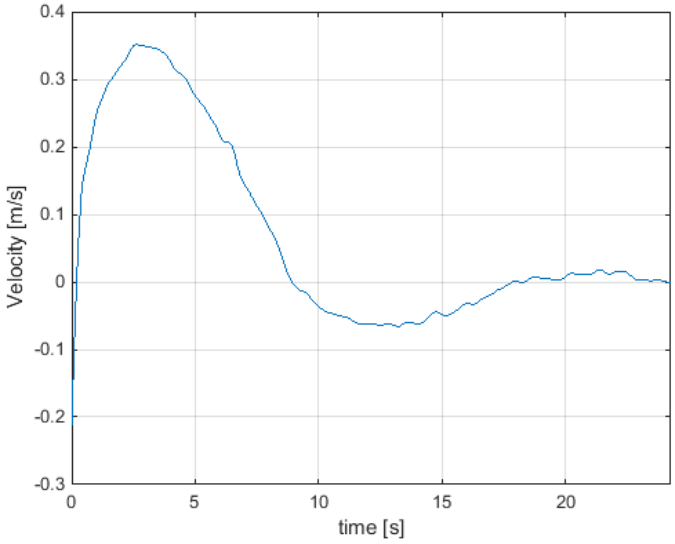

Figure 21. Velocity of the THAUS AUV during trials in the *surge* DOF

The results of the identification task for the THAUS AUV are summarized in Table 13. Even though these results seem good, the THAUS AUV operates at a faster velocity regime, more related to the velocities at which the SCE test was carried out.

Table 13. Hydrodynamic Coefficients of the THAUS AUV Using the Free Decay Pendulum Technique

Parameter	**Value**	**Units**
X_u	-45.7734	kg/s
$X_{\dot{u}}$	-87.1206	kg
Y_v	-93.8563	kg/s
$Y_{\dot{v}}$	-280.7926	kg
Z_w	-49.0414	kg/s
$Z_{\dot{w}}$	-161.1732	kg

C. REMUS AUV RESULTS

The REMUS vehicle tested here does not have an INS. Consequently, a different method was needed to measure the orientation and angular velocity of the pendulum.

Data from the IMU of the Pixhawk Px4 autopilot was used just as the INS data for the THAUS AUV.

A particular property of the REMUS AUV is the considerable difference on its geometry between its principal planes of symmetry. While the *xy-plane* and the *xz-plane* are very similar, having the semi-elliptical shape given by the Myring hull profile equations for a minimal drag coefficient given a length/diameter ratio [2], the *yz-plane* has a circular profile. Due to this fact, the results corresponding to the *surge* DOF are expected to be significantly different from the results in the *sway* and *heave* DOFs.

The results of this test in the *surge* direction are shown in Table 14 as well as the graphical comparison in Figure 22, Figure 23 and Figure 24 for the different damping models

Table 14. Comparison between damping models for *surge* DOF of the REMUS AUV

Damping Model	$X_{\dot{u}}$	X_u	$X_{u\|u\|}$	RMSE
Linear and Quadratic	-39.4273	-7.0972	-18.9418	0.1141
Linear	-39.8851	-13.2476	--	0.1151
Quadratic	-39.8988	--	-36.1892	0.1539

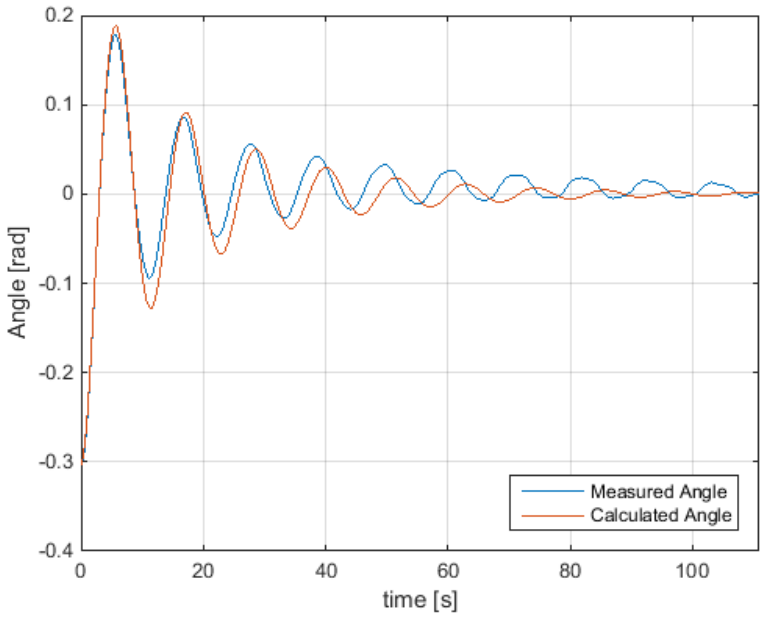

Figure 22. Measured vs. calculated orientation of the REMUS AUV with a linear and quadratic damping model in the *surge* DOF

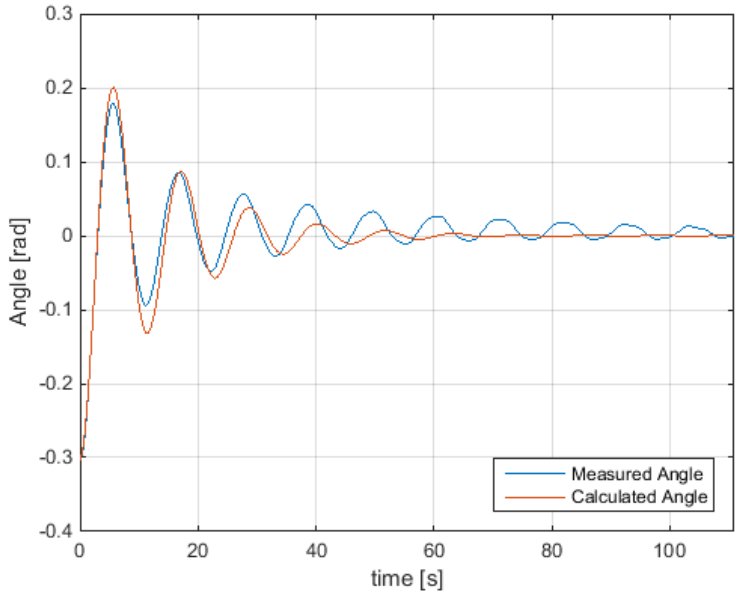

Figure 23. Measured vs. calculated orientation of the REMUS AUV with a linear damping model in the *surge* DOF

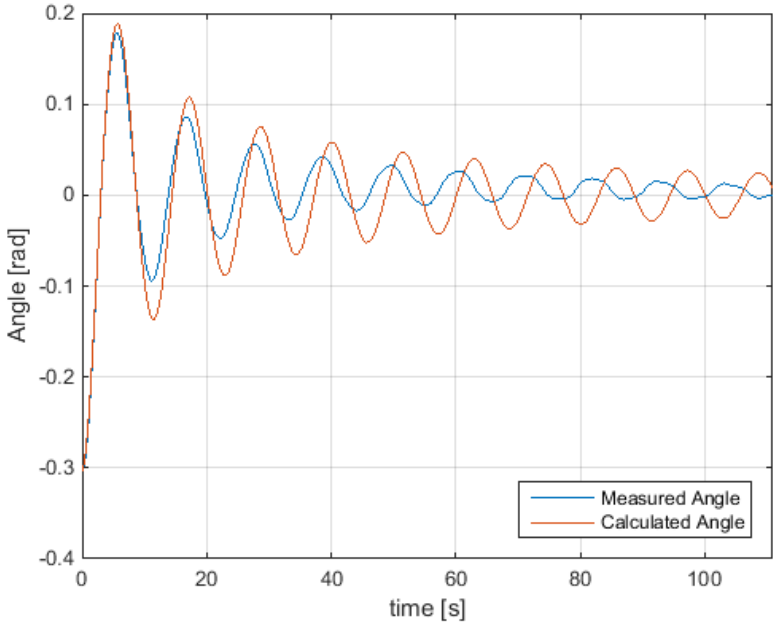

Figure 24. Measured vs. calculated orientation of the REMUS AUV with a quadratic damping model in the *surge* DOF

Figure 25 shows the velocity vs. time of the REMUS AUV during the *surge* DOF test. The maximum speed achieved by the vehicle in this trial was 0.5099 m/s.

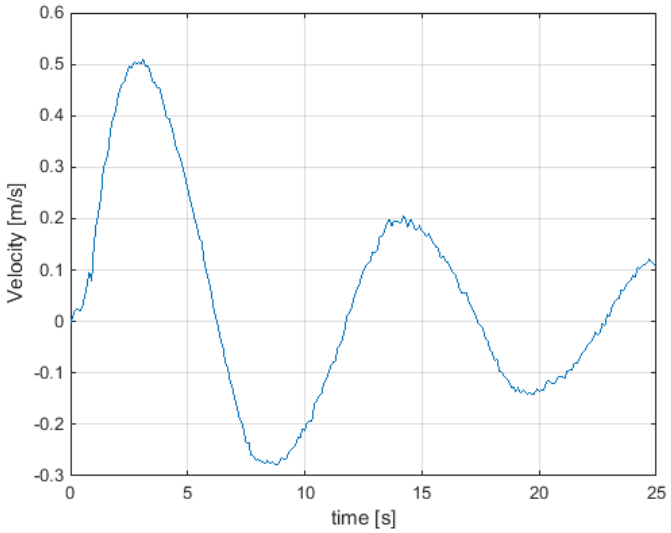

Figure 25. Velocity of the REMUS AUV during trials in the *surge* DOF

As seen for the THAUS AUV, the linear and quadratic damping model dominated over the other two. However, the motion in the *surge* oscillated significantly more than the other DOFs, as will be seen later in this section.

As was also observed for the FDP test of the THAUS AUV, the speed at which this test was carried out for REMUS AUV was not close to the speed at which the vehicle operates (up to 2.3 m/s [19]). Hence, the model obtained using this method is not suitable for real operations of the REMUS.

The same methodology was follow for the *sway* DOF. The comparison between models is summarized in Table 15, Figure 26, Figure 27 and Figure 28.

Table 15. Comparison between damping models for *sway* DOF of the REMUS AUV

Damping Model	$Y_{\dot{v}}$	Y_{v}	$Y_{v\|v\|}$	RMSE
Linear and Quadratic	-178.3699	-93.4415	-14.6473	0.0809
Linear	-178.7444	-96.8761	--	0.0809
Quadratic	-345.9049	--	-285.5404	0.2466

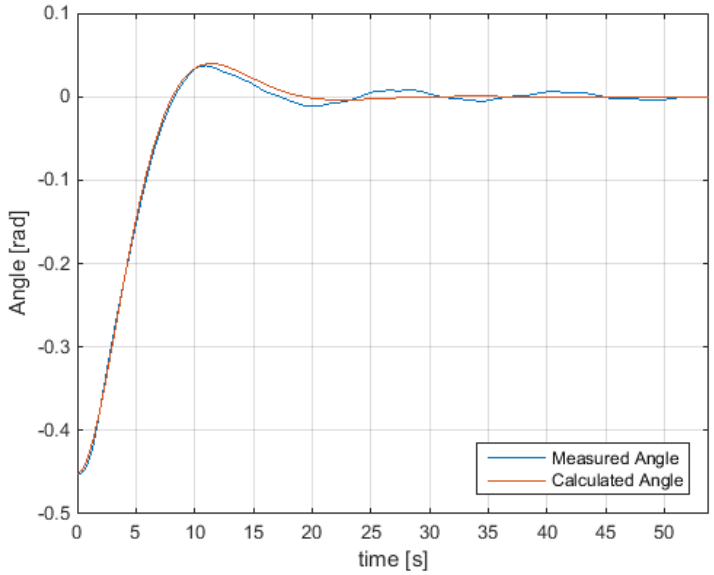

Figure 26. Measured vs. calculated orientation of the REMUS AUV with a linear and quadratic damping model in the *surge* DOF

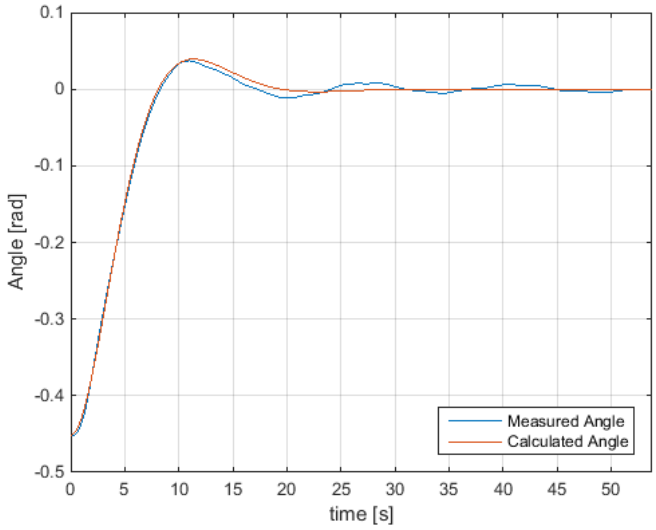

Figure 27. Measured vs. calculated orientation of the REMUS AUV with a linear damping model in the *surge* DOF

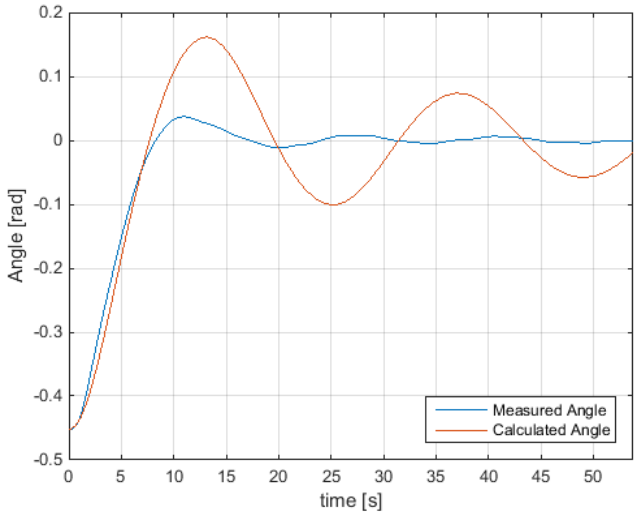

Figure 28. Measured vs. calculated orientation of the REMUS AUV with a quadratic damping model in the *surge* DOF

Figure 29 shows the velocity over time of the REMUS AUV in the *sway* DOF during testing. The maximum speed achieved in this test was 0.3073 m/s.

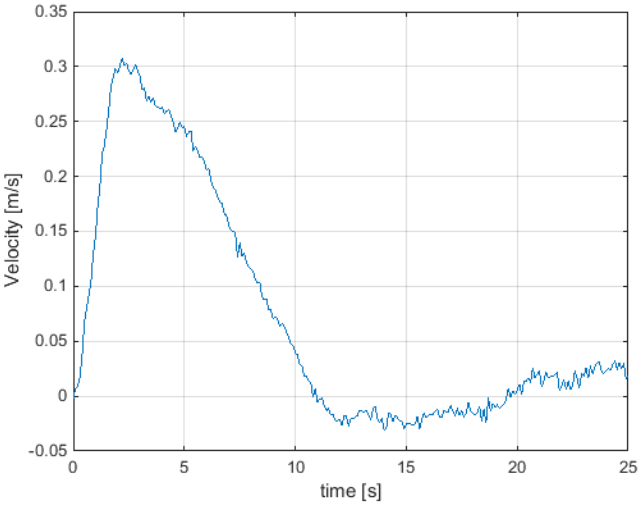

Figure 29. Velocity of the REMUS AUV during trials in the *sway* DOF

As mentioned before, the motion on the *sway* and *heave* DOFs of the REMUS AUV is coupled to the motion of the *surge* DOF. Therefore, small speeds are expected in

the coupled motions. Taking this into consideration, it is expected that the models obtained using the FDP method will work for the *sway* and *heave* DOFs.

The results that best fitted the velocity profile found on this test are summarized in Table 16.

Table 16. Hydrodynamic Coefficients of the REMUS AUV Using the Free Decay Pendulum Technique

Parameter	Value	Units
X_u	-7.0972	kg/s
$X_{u\|u\|}$	-18.9418	kg/m
$X_{\dot{u}}$	-39.8851	kg
Y_v	-96.8761	kg/s
$Y_{\dot{v}}$	-178.7444	kg
Z_w	-91.1800	kg/s
$Z_{\dot{w}}$	-139.1402	kg

THIS PAGE INTENTIONALLY LEFT BLANK

VII. COMPARISON OF METHODS

The two identification methods used in this thesis, Single Channel Excitation (SCE) and Free Decay Pendulum (FDP), were used in the THAUS AUV in order to identify the hydrodynamic coefficients of the vehicle. In this chapter, the results of these two methods will be compared and discussed. The coefficients that best fit the velocity profile of the vehicle in their respective tests are summarized in Table 17.

Table 17. Summary of identified parameters of the THAUS AUV using the SCE and the FDP test

Parameter	SCE	FDP	Units
X_u	--	-45.7734	kg/s
$X_{u\|u\|}$	-132.2436	--	kg/m
$X_{\dot{u}}$	-91.7507	-87.1206	kg
Y_v	--	-93.8563	kg/s
$Y_{v\|v\|}$	-357.8624	--	kg/m
$Y_{\dot{v}}$	-205.0403	-280.7926	kg
Z_w	-85.9259	-49.0414	kg/s
$Z_{w\|w\|}$	--	--	kg/m
$Z_{\dot{w}}$	-194.9859	-161.1732	kg
$N_{r\|r\|}$	-5.8274	--	$\mathrm{kg\,m^2/rad^2}$
$N_{\dot{r}}$	-2.4765	--	$\mathrm{kg\,m^2/rad}$

Since the identification task was carried out on this vehicle without any prior knowledge of the parameters of the plant, is not possible to compare the results to an exact result.

One of the possible reasons for the discrepancy in the result was the lack of Persistence of Excitation (PE) in the FDP test. PE is a very important consideration in order to guarantee convergence of the parameters to the true value, as proven in Section D of Chapter III where the result using a step input was compared to the result having a

series of steps. While both results simulated a similar velocity profile to the original velocity, the identified parameters did not converge to the true values. As a consequence, the results from the SCE are expected to be more accurate.

Another possible reason was that the speed achieved by the tested vehicles during the FDP test was small. The damping in the system is sensitive to the speed. Linear damping is typically associated with laminar flow (low-speed), whereas quadratic damping is associated with higher speed operations. For the FDP test, the speeds were low, and thus it was expected that the linear damping term dominated. However, for the SCE test, vehicle speeds were higher, and as a consequence the quadratic damping term dominated. Since the vehicle is operated in the manner that is consistent with the SCE method, again those results were expected to be more accurate.

In the case of the REMUS AUV, the same was expected for the results on the *surge* DOF, since the speeds at which it operates are even higher than the THAUS operational speeds. However, low speeds are expected for the *sway* and *heave* DOFs, since these are coupled. Therefore, the models obtained using this method in the *sway* and *heave* DOFs are expected to work accurately.

VIII. CONCLUSION

A. SUMMARY

The objective of this research was the identification of the hydrodynamic parameters of the simplified version of the EOM for the THAUS AUV and the REMUS AUV. A Recursive Least Square Estimator (RLSE) was used in conjunction with a parameter estimation technique in both tests used in this research in order to identify the unknown coefficients.

The inertia properties of the vehicles were identified using a quadrifilar pendulum. The relation between the natural frequency of the pendulum and its moment of inertia was used to calculate the later by measuring the period between oscillations and latter subtracting it from the moment of inertia obtained when the vehicle was on top. This was repeated for the three principal planes of each vehicle.

The Single Channel Excitation (SCE) was used in the THAUS AUV due to its ability to excite individual channels at the time. By recording the velocity over time of the vehicle and feeding this information to the regression tools mentioned above, the hydrodynamic parameters for each tested degree of freedom (*surge, sway, heave* and *yaw*) were successfully identified.

The Free Decay Pendulum (FDP) was used in both the THAUS AUV and the REMUS AUV. The identified parameters using this technique differ from the ones identified using the SCE test on the THAUS AUV. Similar results were obtained during simulation of the regression tools, where the results of a Persistently Exciting (PE) input were compared to the results of a non-PE input. This led to conclude that the motion produced by the free decay oscillation of the pendulum is not a PE input. Nevertheless, the resulting model can be used in controllers designed to operate in a low velocity regime.

B. FUTURE WORK

Modeling is an arduous task, but it is required for the design of precise controllers, capable of govern the controlled AUV under complex missions. A full model of the dynamics of the THAUS AUV is required in order to increase its performance under complex tasks. Hence, the SCE test must be carried on in the *roll* and *pitch* DOFs in order to complete the identification task in the vehicle. Later, a verification of the full coupled model must be performed.

The FDP test was concluded to not have a PE input that would lead to the identification of the true hydrodynamic coefficients. However, an external excitation could be introduced in this experimental setup, and as long as this excitation is quantified, regression methods can be used to identify the hydrodynamic parameters. Moreover, the addition of a torsional pendulum would make possible the identification of vehicles like the REMUS AUV, without the capability of individual channel excitation, in the three rotational DOFs (*roll, pitch* and *yaw*).

APPENDIX . SIMULINK MODELS

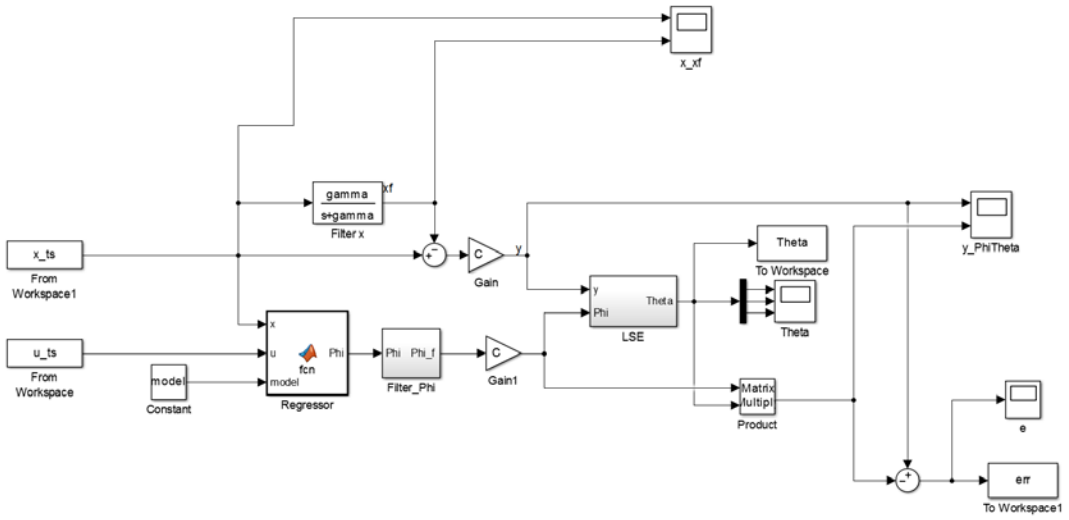

Figure 30. Parameter estimator and recursive least squares estimator diagram.

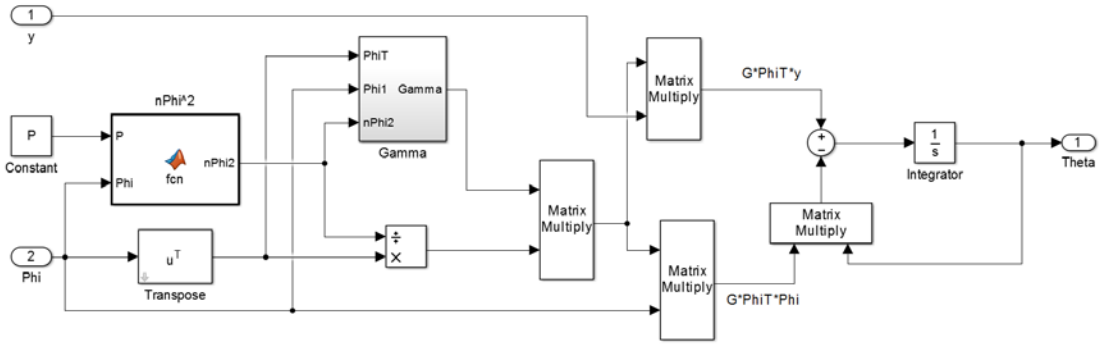

Figure 31. Recursive least square diagram.

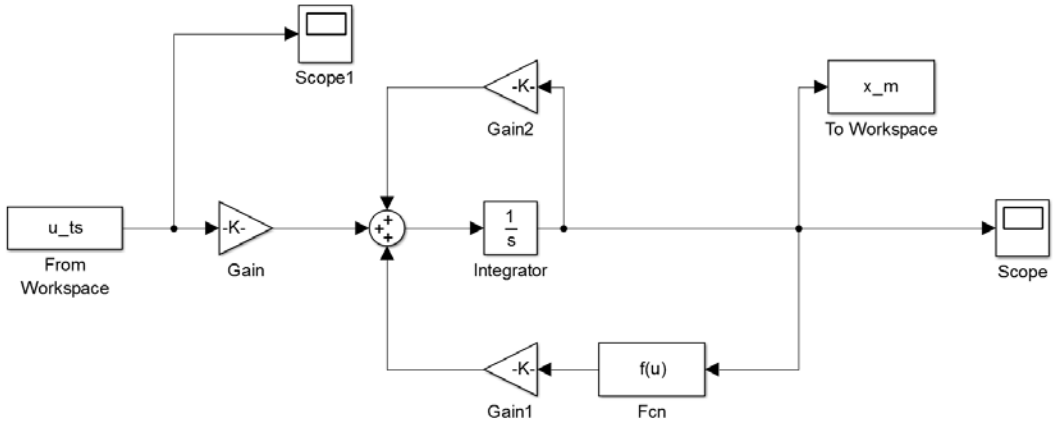

Figure 32. Velocity response simulator for the SCE test

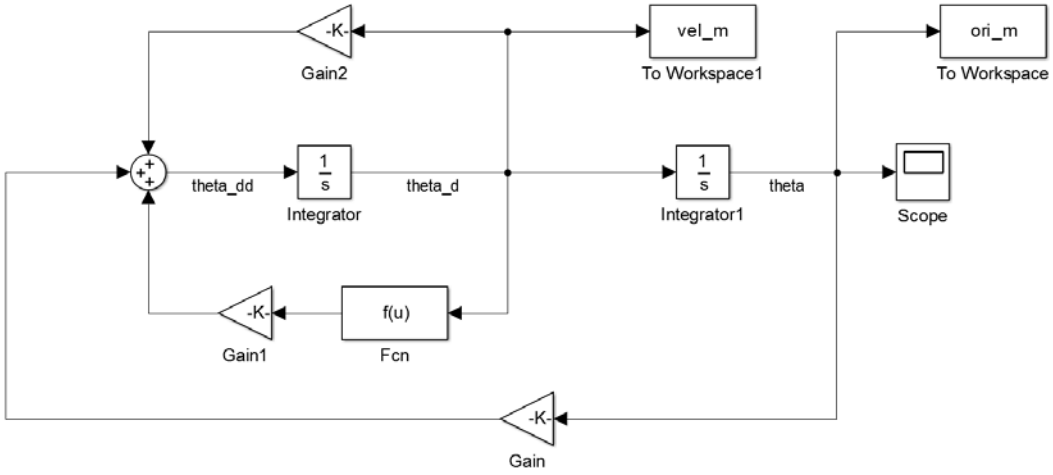

Figure 33. Velocity response simulator for the FDP test

LIST OF REFERENCES

[1] T. I. Fossen, *Guidance and Control of Ocean Vehicle.* New York: Wiley, 1994.

[2] T. Prestero, "Verification of a six-degree of freedom simulation model for the REMUS autonomous underwater vehicle," M.S. Thesis, Dept. Mech. Eng., MIT, Cambridge, MA, 2001.

[3] S. Doherty, "Cross body thruster control and modeling of a body of revolution autonomous underwater vehicle," M.S. Thesis, Dept. Mech. Eng., NPS, Monterey, CA, 2011.

[4] J. Weiss, "Real-time dynamic model learning and adaptation for underwater vehicles," M.S. Thesis, Dept. Mech. Eng., NPS, Monterey, CA, 2013.

[5] Y. Eng, C. Chin and W. Lau, "Added mass computation for control of an open-frame remotely-operated vehicle: application using WAMIT and matlab," *J. Mar. Sci. Technol. -Taiwan,* vol. 22, pp. 405–416, Mar. 2014.

[6] Y. Eng, W. Lau, E. Low and G. Seet, "Identification of the hydrodynamics coefficients of an underwater vehicle using free decay pendulum motion," in *International Multiconference of Engineers and Computer Scientists*, Hong Kong, China, 2008, pp. 1244-1249.

[7] G. Genta and C. Delprete, "Some considerations on the experimental determination of the moments of inertia," *Meccanica,* vol. 29, pp. 125–141, 1994.

[8] X. Chen, J. Chase and P. Wolm, "System identification and modelling of front wheel drive electric wheelchairs," unpublished.

[9] M. Caccia, G. Indiveri and G. Veruggio, "Modeling and identification of open-frame variable configuration unmanned underwater vehicles," *IEEE J. Ocean. Eng.*, vol. 25, pp. 227- 240, 2000.

[10] S. Martin and L. Whitcomb, "Preliminary experiments in comparative experimental identification of six degree-of-freedom coupled dynamic plant models for underwater robot vehicles," *IEEE International Conference on Robotics and Automation,* Karlsruhe, Germany, 2013, pp. 2962–2013.

[11] K. Tan, A. Anvar and T. Lu, "Autonomous underwater vehicle dynamics modeling and performance evaluation," *World Academy of Sci., Eng. and Technology*, vol. 6, pp. 589–597, 2012.

[12] N. Valladarez, "An adaptive approach for precise underwater vehicle control in combined robot-diver operations," M.S. Thesis, Dept. Mech. Eng., NPS, Monterey, CA, 2015.

[13] E. Konstantinidis, “Added mass of a circular cylinder oscillating in a free stream,” *Proc. R. Soc. A-Math. Phys. Eng. Sci.*, vol. 469, Art. No. 20130135, Aug. 2013.

[14] R. D. Blevins, *Formulas for Natural Frequency and Body Shape*. Malabar, FL: R. E. Krieger, 1984.

[15] J. N. Newman, *Marine Hydrodynamics.* Cambridge, MA: MIT Press, 1977

[16] P. Egeskov, A. Bjerrum, C. Aage, A. Pascoal, C. Silvestre and L. Smitt, “Design, construction and hydrodynamic testing of the AUV MARIUS,” in *Symposium on Autonomous Underwater Vehicle Technology*, Cambridge, MA, 1994, pp. 199–207.

[17] K. Åström and B. Wittenmark, “Real-time parameter estimation,” in *Adaptative Control*, 2nd Edition. Boston, MA: Addison-Wesley Longman Pub. Co., 1995, p. 41.

[18] SeaBotix Inc. vLBV300 MiniROV System. [Online]. Available: http://www.seabotix.com/products/pdf_files/vLBV300.pdf

[19] Hydroid – Kongsberg Maritime, “REMUS 100 Autonomous Underwater Vehicle,” [Online]. Available: http://www.km.kongsberg.com/ks/web/nokbg0397.nsf/AllWeb/61E9A8C492C51D50C12574AB00441781/$file/Remus-100-Brochure.pdf?OpenElement

[20] S. Leon, *Linear Algebra with Application*. New Jersey: Pearson Education, 2010.

INITIAL DISTRIBUTION LIST

1. Defense Technical Information Center
   Ft. Belvoir, Virginia

2. Dudley Knox Library
   Naval Postgraduate School
   Monterey, California